University of
South-Eastern Norway

www.usn.no

FMH606 Master's Thesis 2023
Industrial IT and Automation

Vertical track geometry identification from IMU data and GNSS data

University of
South-Eastern Norway

Ruben Svedal Jørundland

Faculty of Technology, Natural Sciences and Maritime Sciences
Campus Porsgrunn

University of
South-Eastern Norway

www.usn.no

Course: FMH606 Master's Thesis 2023
Title: *Vertical track geometry identification from IMU data and GNSS data*
Pages: *57*

Keywords: *Railroad track elevation, Superelevation diagram, Clothoid estimation, IMU and GNSS*

Student: *Ruben Svedal Jørundland*
Supervisor: *Håkon Viumdal, Ole Magnus Brastein*
External partner: *Cemit (Sigurd Aanesen)*

Summary:
This report presents a study on predicting the elevation of a stretch of railroad track using a combination of sensors, data processing techniques, and algorithms. Initially, the research aimed to utilize both an IMU sensor and a GNSS sensor. However, due to noise and filtering issues in the IMU data, the study focused solely on the GNSS sensor.

The investigation involved preprocessing the data, addressing uncertainties in the dataset, and generating clothoid splines to fit the data accurately. Two algorithms, RANSAC and Monte Carlo, were explored for generating clothoids. The simpler RANSAC algorithm combined with optimization achieved the best results, consistently yielding an RMSE below 0.2 meters.

The performance of the solution is primarily dependent on the quality of the input data and its alignment with the actual elevation values. Challenges faced in the study, such as the distribution of points in the clothoid generation process and the lack of a reliable reference for validating the dataset, indicate potential areas for improvement in future research.

In summary, the report demonstrates the feasibility of accurately predicting railroad track elevation using sensors and data processing techniques, while also highlighting the need for further investigation to address the identified limitations and uncertainties.

The University of South-Eastern Norway accepts no responsibility for the results and conclusions presented in this report.

Preface

This thesis investigates the feasibility of utilizing a combination of sensors, data processing techniques, and algorithms to accurately predict the elevation of a stretch of railroad track. The initial approach considered using an Inertial Measurement Unit (IMU) sensor in tandem with a Global Navigation Satellite System (GNSS) sensor to achieve the desired outcome. However, the analysis of initial results led to a change in direction, with the IMU sensor being excluded due to its noise and filtering issues.

The focus of this work is divided into three main components: preprocessing of the data collected, examining the uncertainties in the dataset, and generating clothoid splines that best fit the data. Through the evaluation of different methodologies and algorithms, we aim to understand the performance of the chosen solution and discuss its implications.

The discussion chapter provides a comprehensive analysis of the performance of the implemented solution, uncertainties in the dataset, the different approaches taken, and the discarded preprocessing techniques. By examining these aspects, we aim to identify the strengths and weaknesses of the solution and highlight areas for potential improvement.

This thesis is intended for readers with a background in engineering, computer science, or related fields, who are interested in understanding the challenges and potential solutions for predicting railroad track elevation using a combination of sensors and data processing techniques.

Porsgrunn, 14th May 2023

Ruben Svedal Jørundland

Contents

Preface 3

Contents 5
List of Figures 6
List of Tables 7

Nomenclature 8

1 Introduction 9
1.1 Current solution for track monitoring 10
1.2 Cemits solution 11
1.2.1 Data Collection 12
1.2.2 Superelevation diagram 13
1.2.3 Generation method 14
1.3 Changes During the development 14
1.4 Note on Intellectual Property and Code Disclosure 14

2 Literature Review 15
2.1 Introduction 15
2.2 Materials and Methods 15
2.3 Identifying the Railway Track Geometry 16
2.4 Conclusions 17

3 Data preparation 18
3.1 Filtering IMU data 18
3.1.1 Complementary filter 18
3.1.2 Low-pass filter 20
3.2 S-Grid transformation 23
3.2.1 Combining multiple runs 25
3.3 Preliminary results 26
3.3.1 Changes due to data quality 29
3.3.2 Solution for data preparation 29

4 Clothoid generation 31
4.1 Random sample consensus 31

4.2 Sequential Monte Carlo RANSAC . . . 33
4.3 Brute force local gradient decent . . . 34

5 Results **36**
5.1 GNSS dataset . . . 36
5.1.1 Uncertainty in the dataset . . . 37
5.2 Clothoid generation . . . 39
5.2.1 Random sample consensus . . . 39
5.2.2 Random sample consensus Monte Carlo . . . 42
5.2.3 Brute force local gradient decent . . . 44

6 Discussion **47**
6.1 Preprocessing . . . 47
6.1.1 Uncertainties in the dataset . . . 47
6.2 Clothoid generation . . . 48
6.3 Fusion of IMU and GNSS . . . 48

7 Conclusion **49**
7.1 Further Work . . . 50
7.2 Acknowledgements . . . 50

Bibliography **52**

A Task description **55**

List of Figures

1.1 Example of the data in a superelevation diagram in CVS format. 13

3.1 Pitch estimate from a complementary filter using different values of τ. . . . 20
3.2 Frequency response of the Bessel, Butterworth, Chebyshev, and Elliptic filters [15] 21
3.3 Step response of Bessel, Butterworth, and Elliptic filters [18]. 22
3.4 Pitch estimate from low-pass filtered accelerometer data for different . . . 23
3.5 Comparison of the data calculated using a complementary filter and the pitch from the superelevation diagram 27
3.6 Comparison of the data calculated using a low-pass filter and the pitch from the superelevation diagram 28
3.7 Comparison of the pitch angle calculated from altitude and the pitch from the superelevation diagram 29

4.1 Code for generating a vector of 4 points. Simplified for illustration purposes. 32
4.2 Resulting population of clothoids after 4 iterations of fitting clothoids. . . 34

5.1 Measured altitude of the track 37
5.2 Standard deviation at each point in the s-grid. 38
5.3 Resulting clothoid spline using 1000 iterations and 50 clothoids on the dataset. 40
5.4 Resulting clothoid spline using 1000 iterations and 85 clothoids on the discretized superelevation diagram. 41
5.5 Close up of Figure 5.4 showing the redundant points. 42
5.6 Resulting clothoid spline using 100 iterations, 50 clothoids, and a population of 1000 on the dataset. 43
5.7 Resulting clothoid spline using 100 iterations, 85 clothoids, and a population size of 1000 on the discretized superelevation diagram. 44
5.8 Comparison between before and after optimization. 45
5.9 Comparison between before and after optimization using the superelevation diagram as input. 46

List of Tables

3.1 Illustration of pitch and altitude data aligned in the s-grid. 25
3.2 Example data-set of altitudes from different runs averaged. 26

Nomenclature

Symbol	**Explanation**
CDC	Cemit Data Collector
IMU	Inertial Measurement Unit
GNSS	Global Navigation Satellite System
RANSAC	Random sample consensus
ODE	Ordinary differential equation
RMSE	Root Mean Square Error

1 Introduction

The accurate prediction of railroad track elevation plays a crucial role in maintaining the safety and efficiency of railway operations. Understanding the elevation profile enables engineers to plan and design appropriate superelevation, manage train speeds, and implement effective maintenance strategies. With the advancements in sensor technology and data processing techniques, there is potential for developing reliable methods to predict the elevation of railroad tracks.

This report aims to investigate the feasibility of utilizing numerous train passes over a section of track to determine the track's elevation by exploring the use of sensors, data preprocessing, and algorithms. Initially, the study sought to combine data from an Inertial Measurement Unit (IMU) sensor and a Global Navigation Satellite System (GNSS) sensor. However, due to issues with noise and filtering in the IMU data, the focus shifted to solely utilizing the GNSS sensor data.

The goal of this solution is to merge data from these train passes with technical drawings of the track to generate a comprehensive elevation map. With this elevation map, a clothoid spline representing the elevation can be created. This approach is founded on previous research conducted in-house at Cemit. The solution seeks to build upon Cemit's work in creating superelevation diagrams by incorporating elevation data into these diagrams, devising a novel approach specifically for this purpose.

The report is structured as follows: First, the data preprocessing stage is discussed, detailing the methods used to clean and process the raw sensor data. This section also addresses the uncertainties in the dataset and the challenges faced in validating the accuracy and precision of the data. Next, the clothoid generation process is examined, including the exploration of two algorithms, RANSAC and Monte Carlo, for generating clothoids to fit the data accurately. The performance of these algorithms and the impact of optimization techniques on their results are analyzed.

Finally, the report concludes with a summary of the findings, a discussion of the limitations and uncertainties encountered during the study, and suggestions for future research directions to improve the prediction of railroad track elevation.

1.1 Current solution for track monitoring

Monitoring railway tracks is crucial for maintaining safety, efficiency, and reliability in railway systems. Various methods are employed to monitor the location and geometry of railway tracks, including both traditional and advanced technologies[1]. Each of these solutions has its own set of advantages and disadvantages, which can make them labor-intensive or require expensive equipment. Here is a brief overview of the mentioned solutions and their challenges:

1. Manual inspections: Traditional inspections involve human operators visually examining the tracks for potential issues such as irregularities, wear, and damage. While this method is relatively low cost, it can be labor-intensive, time-consuming, and subject to human error. A significant number of personnel are required to cover vast stretches of railway tracks, and human operators may not be as efficient or accurate as automated systems, leading to potential errors and inconsistencies in the inspection process.

2. Track Geometry Measurement Systems[2] (TGMS): These systems use a set of sensors and equipment mounted on a dedicated measurement train or a vehicle running on the tracks. The TGMS collects data on various parameters, such as track gauge, alignment, cross-level, and curvature. The collected data is then analyzed to identify deviations from the standard track geometry, which might require maintenance or repairs. While TGMS can provide accurate and detailed information about track geometry, the required sensors and equipment can be expensive to acquire, install, and maintain. Dedicated measurement trains or vehicles need to be periodically deployed, which can disrupt regular train schedules and require additional personnel to operate and analyze the collected data.

3. LiDAR-based systems: LiDAR (Light Detection and Ranging) is a remote sensing technology that uses laser light to measure distances and create high-resolution digital models of the environment. LiDAR-based systems can be mounted on trains, vehicles, or drones to collect precise data on track geometry, including the location of the tracks, curvature, and alignment. This method provides more accurate and faster data collection compared to manual inspections. However, the equipment needed for LiDAR-based systems, such as laser scanners and high-precision GPS, can be costly. Mounting the equipment on trains, vehicles, or drones may require specialized expertise and infrastructure. While LiDAR systems are less labor-intensive than manual inspections, they still require skilled personnel to analyze and interpret the collected data[3].

4. Ground Penetrating Radar (GPR): GPR is a non-destructive testing method that uses radar pulses to create images of subsurface structures. GPR can detect subsurface defects, such as voids or cracks, which might compromise the track's structural

integrity. This method can be used in combination with other monitoring techniques to provide a comprehensive assessment of track conditions. GPR systems can provide valuable information about subsurface structures and defects, but the equipment can be expensive, especially for high-resolution and deep-penetration radar systems. GPR surveys may also require track closures or slow-moving trains, making them time-consuming and potentially disruptive. Moreover, the interpretation of GPR data can be complex and requires skilled personnel with expertise in radar data processing and subsurface geophysics[4].

1.2 Cemits solution

Cemit is a company that concentrates on providing low-cost and easy to install solutions for railway monitoring. Their strategy involves gathering a large amount of sub-optimal data over extended periods instead of smaller data-sets of high-quality data. However, due to the low quality of data, more data processing and data science is required to extract useful insights.

For effective data utilization and accurate prediction of the railway's condition, Cemit necessitates a mathematical model that represents the railway track. This model can be constructed using a superelevation diagram[5] corresponding to the specific railway segment. By consolidating measured data collected from trains traveling along the designated railway section and conducting simulations with the mathematical model, a range of track parameters can be determined. Nevertheless, the success of this technique is contingent upon the accuracy of the track model.

The precision and availability of superelevation diagrams pose significant obstacles to this approach. Acquiring superelevation diagrams is challenging because they are not openly accessible to the public for unrestricted examination. Moreover, the aging railway infrastructure often renders these diagrams obsolete, as they do not consider any alterations do to movements in the ground and updates often only happen during overhauls to the track. Although it is possible to manually amend inaccuracies in the superelevation diagrams with the assistance of satellite images, this method is labor-intensive and lacks scalability for analyzing longer sections of railway track. Consequently, alternative solutions may be required to address these limitations and improve the overall effectiveness of the approach.

To address the issue of outdated superelevation diagrams and enable predictions for track sections where these diagrams are unavailable, Cemit aims to generate them from data. Work has already begun on this initiative, with the development of a prototype capable of creating a 2-dimensional superelevation diagram using GNSS data from trains traversing a specific track segment. However, this solution assumes that the track lies on a perfectly flat surface. While it may be effective for shorter track sections on relatively flat terrain, the accuracy diminishes as the track length increases.

To tackle this challenge, Cemit plans to explore the possibility of extending this solution to incorporate elevation data. The objective is to produce superelevation diagrams precise enough for track analysis purposes. In order to accomplish this goal within a reasonable time frame and minimize the impact on the existing data infrastructure used for predicting superelevation diagrams, the proposed approach involves augmenting the already generated diagrams with elevation data. This method is selected to prevent the need for a complete overhaul of the current solution. Instead, the updated solution will utilize the output from the existing solution, integrate elevation information, and generate a new 3-dimensional superelevation diagram.

1.2.1 Data Collection

In order to accomplish this objective, Cemit utilizes a data collector mounted within the train cabin. The Cemit Data Collector (CDC) records acceleration, angular velocity, and GNSS data. This approach allows for continuous data recording while the train is in motion. However, this also contributes to lower data quality, as the measurements include the effects of the train's suspension.

The CDC is outfitted with an MPU6050 inertial measurement unit, which captures linear acceleration and angular velocities in three dimensions at a 400 Hz sampling rate. It records acceleration within a range of $\pm 2g$ and angular velocity within a range of $\pm 500°/sec$ using a 16-bit register, resulting in resolutions of $0.00006103515g$ and $0.00762939453°/sec$, respectively [6]. Additionally, the CDC is equipped with a Quectel EC25-E, which serves as the GNSS sensor. It samples position and altitude at a 5 Hz rate using the GLONASS and GPS satellite networks [7].

Trains as drones

One of Cemit's objectives is to leverage existing trains already in operation on the tracks as sensors. Passenger and freight trains traverse the track infrastructure daily. By utilizing these trains as sensors, the railway can be monitored nearly continuously. To achieve large-scale deployment, the installation of sensor equipment must be straightforward. This is why the CDC is used and mounted inside the train cabin. Installing sensors on the train's undercarriage would yield superior data quality but would result in a significantly more expensive and complicated installation process.

1.2.2 Superelevation diagram

A superelevation diagram encompasses all parameters of the track geometry. The geometry is divided into three primary components, which are:

1. Horizontal geometry: The curvature of the railway along the horizontal plane.
2. Vertical geometry: The curvature of the railway along the vertical plane.
3. Superelevation height: The difference between the inner and outer rails of the track. This is used to compensate for the forces experienced when the track curves in the horizontal plane [8].

These parameters describe multiple clothoid splines linked together to form the track. An example of such a diagram is shown in Figure 1.1, where each line represents a location where the track's curvature changes.

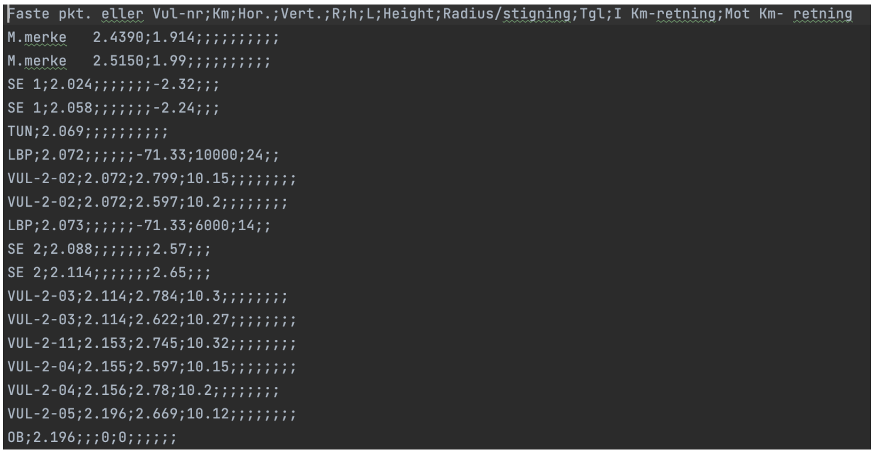

```
Faste pkt. eller Vul-nr;Km;Hor.;Vert.;R;h;L;Height;Radius/stigning;Tgl;I Km-retning;Mot Km- retning
M.merke   2.4390;1.914;;;;;;;;;;
M.merke   2.5150;1.99;;;;;;;;;;
SE 1;2.024;;;;;;;-2.32;;;
SE 1;2.058;;;;;;;-2.24;;;
TUN;2.069;;;;;;;;;;
LBP;2.072;;;;;;-71.33;10000;24;;
VUL-2-02;2.072;2.799;10.15;;;;;;;;
VUL-2-02;2.072;2.597;10.2;;;;;;;;
LBP;2.073;;;;;;-71.33;6000;14;;
SE 2;2.088;;;;;;;2.57;;;
SE 2;2.114;;;;;;;2.65;;;
VUL-2-03;2.114;2.784;10.3;;;;;;;;
VUL-2-03;2.114;2.622;10.27;;;;;;;;
VUL-2-11;2.153;2.745;10.32;;;;;;;;
VUL-2-04;2.155;2.597;10.15;;;;;;;;
VUL-2-04;2.156;2.78;10.2;;;;;;;;
VUL-2-05;2.196;2.669;10.12;;;;;;;;
OB;2.196;;;0;0;;;;;;
```

Figure 1.1: Example of the data in a superelevation diagram in CVS format.

Superelevation diagrams are represented in various formats, but they typically share the same parameters. These parameters have different names across formats. Additionally, many of the diagrams include extra parameters, such as points of interest along the track. However, the critical parameters are as follows:

1. sh: Distance of the spline in the horizontal plane, in meters.
2. rh: Radius of the splines in the horizontal plane, in meters.
3. sv: Distance of the spline in the vertical plane, in meters.
4. rv: Radius of the splines in the vertical plane, in meters.
5. h: Height difference of the inner and outer cord, in millimeters.

1.2.3 Generation method

In order to create accurate superelevation diagrams, it is advised to combine data from both IMU and GNSS sources. This process involves fusing elevation information from the GNSS with angle estimates from the IMU, resulting in a detailed dataset for each train run over the track. By averaging multiple runs, a dataset representing the track's elevation can be generated. A spline can be fitted to this data and used as a mathematical model, or its parameters can be extracted to develop a new superelevation diagram.

1.3 Changes During the development

During the course of this project, some modifications were made to the original plan to facilitate the development of an effective solution within a reasonable time frame. The initial intention was to fuse IMU data with GNSS data, but the decision was made to focus solely on GNSS data. This allowed for more time to refine the solution and to include the generation of a clothoid spline from the GNSS data. This decision was made because it was determined that attempting to fuse GNSS and IMU data would have consumed a considerable amount of time with a low likelihood of improving the outcome.

1.4 Note on Intellectual Property and Code Disclosure

It is important to address the absence of specific implementation details and code examples in the report. The reason for this omission is that parts of the solution described in this study is currently in the process of being patented. As a result, to protect the intellectual property rights and ensure the novelty of the solution, the code and certain implementation details cannot be disclosed at this time.

Once the patent application has been granted, more detailed information regarding the solution, including code examples and implementation specifics, may become available. However, for the time being, the report will focus on the general principles, algorithms, and methodologies used to achieve the stated goals, without divulging sensitive information that may compromise the patent application process.

2 Literature Review

Title: Preparatory Railway Track Geometry Estimation Based on GNSS and IMU Systems[9].
Authors: Slawomir Judek, Andrzej Wilk, Wladysław Koc, Leszek Lewiński, Artur Szumisz, Piotr Chrostowski, Sławomir Grulkowski, Jacek Szmagliński, Michal Michna, Krzysztof Karwowski, Jacek Skibicki, and Roksana Licow
Institution: Gdańsk University of Technology

The importance of accurately determining railway track geometry is well established in the literature, and various methodologies have been proposed to achieve this goal. The study by Judek et al. explores the use of Global Navigation Satellite System (GNSS) and Inertial Measurement Unit (IMU) technology for estimating railway track geometry.

2.1 Introduction

The introduction provides an overview of the current state of railway track geometry estimation and highlights the challenges faced by traditional geodetic methods, such as time-consuming processes and imprecise results. The authors emphasize the need for an efficient and accurate methodology to estimate railway track geometry and propose the integration of GNSS and IMU technologies.

2.2 Materials and Methods

The authors present a comprehensive description of the equipment and experimental setup employed in their study. They utilize two high-frequency (20 Hz) GNSS receivers in combination with a high-precision IMU system to collect and process data for track geometry estimation. The GNSS receivers are responsible for providing positional data, while the IMU system measures angular velocities and accelerations, as well as lateral and longitudinal inclination angles of the railway track.

The experimental setup involves the installation of the GNSS receivers and IMU system on a mobile platform, allowing the collection of data while traversing the railway track.

This mobile configuration enables the continuous acquisition of data, which is crucial for accurate track geometry estimation.

For post-processing the GNSS data, specialized software is used to correct for various error sources, such as satellite clock and orbital errors, atmospheric delays, and multipath effects. This software also enables the calculation of the base vector, which is a useful quality indicator for the obtained results.

In addition to the GNSS data post-processing, the authors also discuss the processing of the IMU data, which involves the application of various filtering algorithms such as Whittaker and Savitzky–Golay filters. These filters are employed to smooth the data and calculate derivatives, enabling the accurate estimation of track geometry elements such as curvature and lateral inclination angles.

Overall, the materials and methods section provides a detailed overview of the experimental setup and data processing methodology employed in the study, showcasing the potential of combining GNSS and IMU systems for railway track geometry estimation.

2.3 Identifying the Railway Track Geometry

In this section, the authors delve into the process of identifying specific railway track geometry elements, such as straight sections, circular arcs, and transition curves, which are crucial for train running parameters. They highlight the challenges of determining railway track curvature from discrete and potentially noisy measurements obtained through GNSS and IMU systems.

A variety of methodologies are explored for calculating and analyzing track curvature, including equations of motion, complex iterative algorithms, and the chord method. The authors emphasize the importance of selecting appropriate filtering and approximation algorithms to account for the quality indicators of the data, as well as the required INS parameters for measuring angles.

The authors present two methods for computing curvature based on the measured coordinates. However, due to the discrete nature of the data and uncertainties associated with measurements, digital data processing is employed to approximate curvature values.

To overcome the challenges in calculating the curvature, the authors employ the Savitzky-Golay algorithm to compute the derivatives and the Whittaker algorithm for filtering. They demonstrate the effectiveness of these algorithms in determining the radii of circular arcs and identifying railway track geometry elements.

Additionally, the authors discuss the use of lateral inclination angle measurements obtained from the IMU/INS system to further support the identification of track geometry elements. By integrating the curvature variability analysis with lateral angle variability analysis, they aim to combine the advantages of both approaches, offering a more accurate and comprehensive track geometry estimation.

In conclusion, the section on identifying railway track geometry highlights the complexities of the task and showcases the benefits of integrating GNSS and IMU measurements with advanced filtering and approximation algorithms. The authors' research aims to develop a data fusion algorithm that automatically reconstructs track geometry from mobile GNSS/INS measurements, supporting design processes and track maintenance performed by railway infrastructure managers.

2.4 Conclusions

Judek et al. conclude that mobile GNSS measurements are a valuable tool for determining and estimating railway track geometry during operation. They recommend the use of high-frequency GNSS receivers with post-processing and the incorporation of IMU/INS units for precise angle measurements. The authors also highlight the potential for further research in developing algorithms that automatically reconstruct track geometry from mobile GNSS/INS measurements to support railway infrastructure management and design processes.

In summary, the study by Judek et al. provides a comprehensive overview of the integration of GNSS and IMU systems for estimating railway track geometry. The experimental results demonstrate the potential of this approach in achieving accurate and efficient track geometry estimation, thereby offering a promising alternative to traditional geodetic methods.

3 Data preparation

Before creating a superelevation diagram with altitude information, it is necessary to undergo preparation, cleaning, and transformation processes. The first step involves gathering data from Cemits databases. This will not be explained in detail, as it is considered basic database querying. However, it is important to note that this is where the data is sourced from.

Data preparation involves several steps, beginning with filtering both IMU and GNSS data for each run over a track segment in the time-domain. Subsequently, the data is transformed into an s-grid e.g the travel distance along the rail (see 3.2). This is to align the x-axis across all runs.

3.1 Filtering IMU data

The goal of filtering the IMU data is to determine the train's pitch angle. This can be achieved by employing a complementary filter[10], which directly provides the angle, or by applying a low-pass filter to the signal and subsequently extracting the angle through trigonometry. Both of these methods for obtaining the angle have been tested and compared to ensure the highest quality data for further processing.

3.1.1 Complementary filter

To extract angle information from the IMU, a complementary filter is employed. This filter fuses the acceleration and angular velocities measured by the IMU to produce an estimate of orientation[11]. In this case, a complementary filter based on Euler angles is chosen, even though it may not be optimal. Euler angles can suffer from gimbal lock, but for the small elevation angles experienced by a train, this should not be a problem [12].

The discrete complementary filter is of the form:

$$\theta[n] = (1-\alpha)(\theta[n-1] + \omega[n] * dt) + \alpha * x[n]$$

$$x[n] = tan^{-1}\left(\frac{-ay[n]}{\sqrt{ax[n]^2 + az[n]^2}}\right)$$

[13]

where:

- θ: pitch angle.
- ω: angular velocity (rad/s).
- x: orientation estimate from linear acceleration.
- α: filter constant.
- dt: time step.
- ax: acceleration component from the x-axis.
- ay: acceleration component from the y-axis.
- az: acceleration component from the z-axis.

Note that in this implementation, α and $(1-\alpha)$ are swapped. The conventional representation of a complementary filter is $\theta[i] = \alpha * v + (1-\alpha) * x[i]$. This means that lower values of α result in higher filtering. The formula is maintained this way to ensure consistency with further results.

To more easily compare the results later, the time-constant τ is used instead of the filter-constant α. α can easily be calculated from τ using the following formula:

$$\alpha = \frac{dt}{dt + \tau}$$

Applying the complementary filter to one run gives the pitch estimate over time. Figure 3.1 shows the pitch estimate of one run over the selected track with different values for τ.

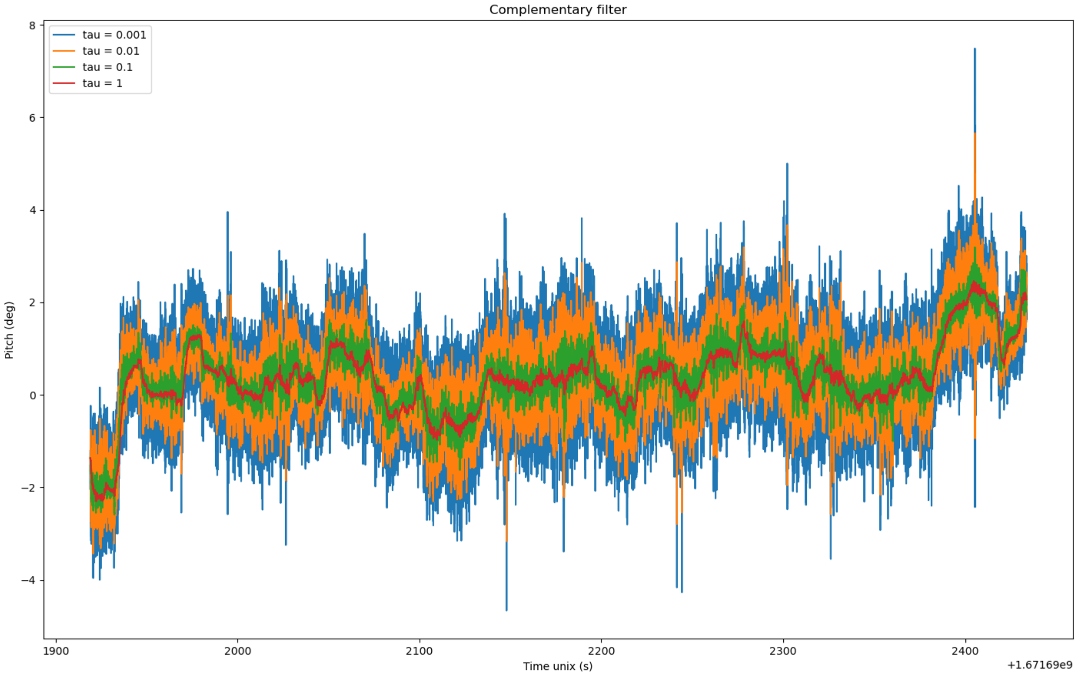

Figure 3.1: Pitch estimate from a complementary filter using different values of τ.

Increasing the time-constant of the complementary filter will enhance the filtering of the signal, as shown in Figure 3.1. Increasing τ also impacts how much the filter ”trusts” the gyroscope or the accelerometer, with $\tau = 0$ relying solely on the accelerometer and $\tau = \infty$ relying exclusively on the gyroscope.

$$\tau = 0 \rightarrow \alpha = 1$$

$$\tau = \infty \rightarrow \alpha = 0$$

3.1.2 Low-pass filter

The pitch angle of the train can be extracted using only the accelerometer. This is achieved by first applying a low-pass filter on the accelerometer signal to remove noise, and then using trigonometry to obtain the angle. This method provides more control over the filtering process, since different filters can be chosen freely. However, it is susceptible to disturbances such as train acceleration.

The first step is filtering the signal. Different filter choices come with their own advantages and disadvantages. The most common trade-off is between cutoff frequency and ripple in the pass-band. Figure 3.2 displays the frequency response of the most common types of IIR filters[14].

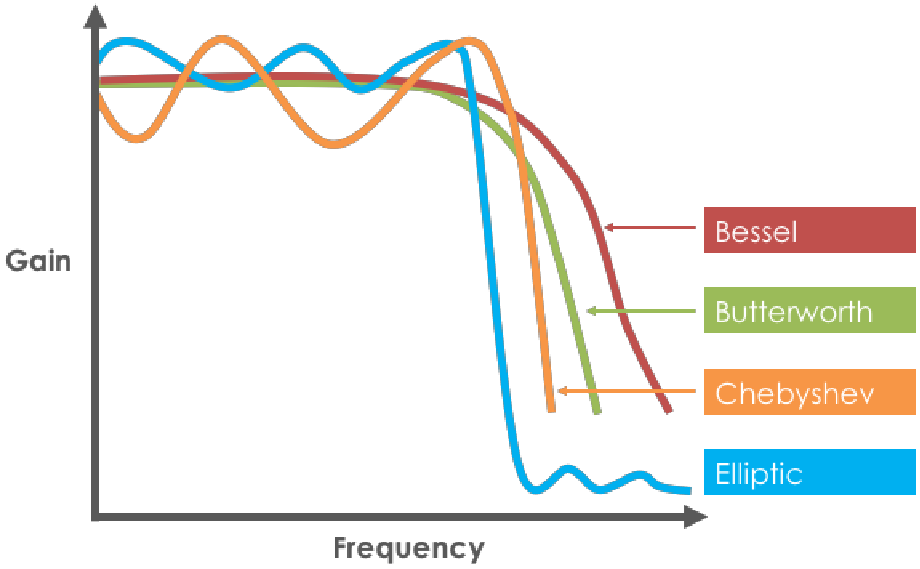

Figure 3.2: Frequency response of the Bessel, Butterworth, Chebyshev, and Elliptic filters [15]

As shown in figure 3.2, Bessel and Butterworth are the 2 filters whit out ripple in the pass-band. However, this is not the only important filter parameter to consider. While the Butterworth filter appears superior when examining the step response, it has one disadvantage that the Bessel filter does not: overshoot in the transient response and subsequent ripple, as shown in Figure 3.3. This overshoot may cause amplification of only some parts of the signal, which is undesirable[16][17].

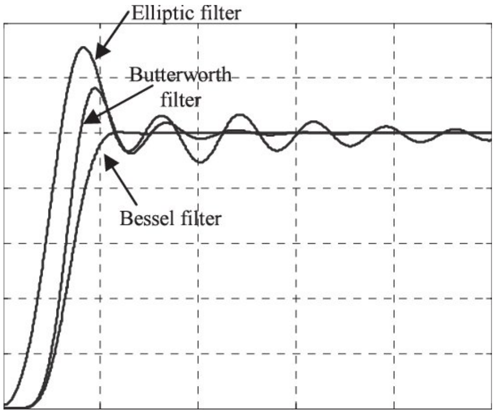

Figure 3.3: Step response of Bessel, Butterworth, and Elliptic filters [18].

Due to these properties, the chosen filter is the Bessel filter. This is the ”laziest” filter, meaning it has a slow cutoff but no other disadvantages.

After filtering, the second step is computing the train’s pitch angle using the filtered signal with the following formula:

$$\theta[i] = \tan^{-1}\left(\frac{-ay[i]}{\sqrt{ax[i]^2 + az[i]^2}}\right)$$

where:

- θ: pitch angle.
- ax: acceleration component from the x-axis.
- ay: acceleration component from the y-axis.
- az: acceleration component from the z-axis.

Practically, this is implemented using Scipy’s filtfilt function [19]. This applies the filter both forward and backward in time, eliminating phase shift, making the filter non-causal. This is only possible since the filtering is performed on a finite signal and not in real-time, sins the backwards pass starts in the ”future” and filters backwards in time. To more easily compare results with the other methods, τ is used to compute the cutoff frequency for the filter.

$$f_c = \frac{1}{2\pi \cdot \tau}$$

where:

- f_c: Cutoff frequency of the filter

From these two steps, an estimate of the orientation can be obtained. Figure 3.4 shows the orientation estimate for different values of tau used for filtering.

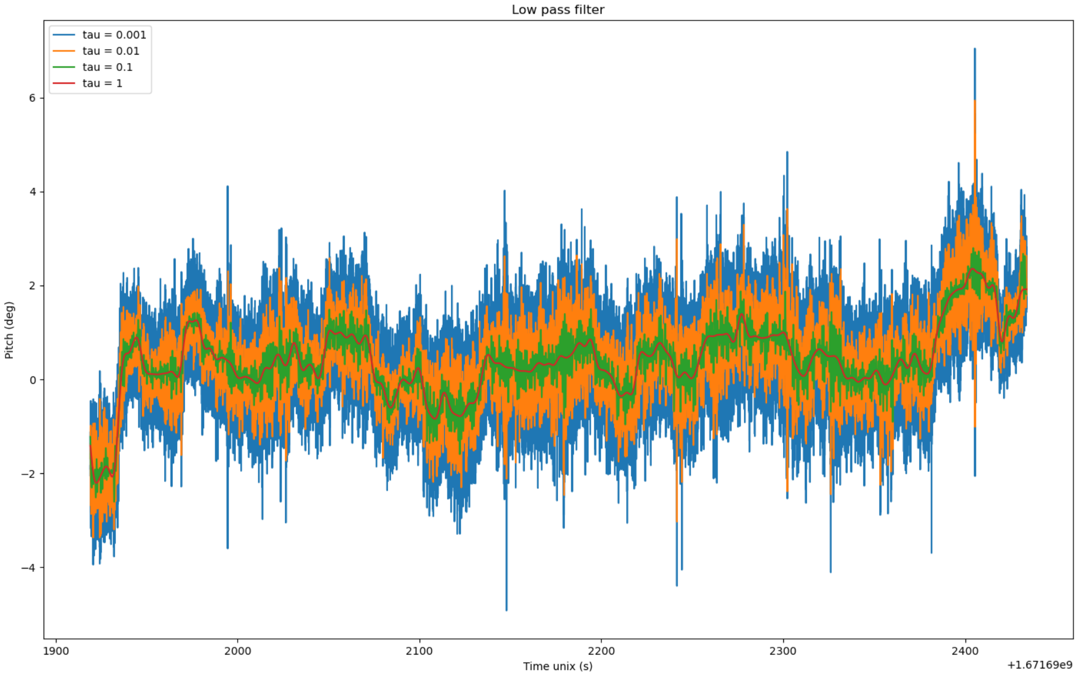

Figure 3.4: Pitch estimate from low-pass filtered accelerometer data for different

3.2 S-Grid transformation

To average over multiple runs, all the runs must be on the same common geometric reference. Time as the reference is not suitable for this due to the train taking different amounts of time for each run. Therefore, averaging multiple runs in this way is not possible. To solve this, each run needs to be transformed onto a common geometric reference, which has been named the ”s-grid”. The axis represents the distance along a set of connected clothoids from start to end, or in other words, the distance along the arc-length of all the clothoids. This is obtained from the superelevation diagram for the given stretch of the track, or it can be estimated by Cemits prototype for creating 2-dimensional clothoid splines.

Computing the s-grid is done by first discretizing all the clothoids in the superelevation diagram for the track. This is achieved by numerically integrating the equations for a clothoid spline.

$$\theta = k(s)$$
$$dx = \sin(\theta)ds$$
$$dy = \cos(\theta)ds$$

where:

- θ: Angle at the given point.
- k: curvature at the given point.
- s: Distance along the spline.
- ds: Step length along the spline.
- k: curvature at the given point.
- x,y: Points in the Cartesian plane

Analytically solving this ODE is complicated due to the changing curvature of the spline and must be done whit numerical integration. However, since the curvature $\frac{d\theta}{ds} = \kappa_0 + \kappa_1 s$ is linear in s, the curvature κ can be trivially computed for any point s in each clothoid segment, which drastically simplifies the problem.

Solving this ODE gives the x and y coordinates of all the points along the spline in the Cartesian plane, where x_0 and y_0 are at coordinate (0,0). The next step is to determine the coordinates of all these points in Earth's coordinate frame. To achieve this, the latitude and longitude of the start of the track must be known. The latitude and longitude of the next point are then estimated with a geodesic transform [20] provided by GeographicLib [21].

Estimating the subsequent point in Earth's coordinate frame is done by calculating the azimuth angle from the current point to the point in the Cartesian plane.

$$dx = x[i+1] - x[i], dy = y[i+1] - y[i]$$
$$d[i] = \sqrt{dx^2 + dy^2}$$
$$\alpha[i] = \tan^{-1}\left(\frac{dy}{dx}\right) \cdot \frac{180}{\pi}$$

where:

- α: Azimuth angle or bearing
- d: Distance

Moving the distance d in the direction α in Earth's coordinate frame gives an approximation of the next point. Repeating this for all the points of the spline in the Cartesian frame gives an approximation of the latitude and longitude of the points in the spline.

With the s-grid computed, the data for different runs can be placed on the same x-axis. For the altitude data, this is quite simple since it comes bundled with latitude and longitude in an NMEA GNSS package [22]. The altitude measurements from the train's GNSS receiver are then placed on the closest position in the s-grid. Pitch data, on the other hand, which is based on filtered IMU data, must first be aligned in time with a GNSS position. This is done by selecting the closest pitch data-point in time to each GNSS measurement. Then the pitch measurements can be aligned on the s-grid in the same way as the GNSS measurements.

Aligning the data along the s-grid creates a table where all the data points are aligned along the distance of the track. An example of such a table is shown in Table 3.1, note that not all rows contain values. Each data point correlates to one GNSS measurement, so it is dependent on the sampling rate of the GNSS receiver.

s	**pitch**	**Altitude**
0	0.01	100
1	NaN	NaN
2	0.02	105
3	NaN	NaN
4	0.02	110
⋮	⋮	⋮
s_n	NaN	NaN

Table 3.1: Illustration of pitch and altitude data aligned in the s-grid.

3.2.1 Combining multiple runs

To obtain a better estimate of the actual values of altitude and pitch along the track, more than one run is needed. With all the runs over the track transformed to the s-grid, their x-axes align. This makes it possible to combine multiple transformed runs to fill out missing data points along the s-grid and obtain an average or median at each point.

The average or median is calculated for each point along the s-axis, ignoring NaN values. Table 3.2 shows an illustration of this for the altitude values, but the same methodology applies to pitch.

s	A1	A2	A3	A_n	A_mean
0	100	NaN	NaN	NaN	100
1	NaN	NaN	105	NaN	105
2	NaN	105	NaN	105	105
$\vdots$	$\vdots$	$\vdots$	$\vdots$	$\vdots$	$\vdots$
s_n	110	NaN	100	NaN	105

Table 3.2: Example data-set of altitudes from different runs averaged.

Note that ignoring NaN values means that the average of 100, 110, and NaN is 105. This combining results in all the points from s_0 to s_n obtaining a value if the number of runs being combined is large enough.

3.3 Preliminary results

With all the data sets transformed into the s-grid and combined, it is possible to get an indication of how the data matches the existing superelevation diagram for the track. This provides insight into whether the data is useful. The superelevation diagram for the track contains the pitch angle of the track as it was when it was built. Comparing this with the combined IMU data shows if there is any correlation in the data. The same can be done with GNSS data, which just needs to be converted from altitude to angle first.

The correlation between the IMU data and the superelevation diagram is not very good. Figure 3.5 shows the correlation using a complementary filter, while Figure 3.6 shows the correlation using the method of low-pass filtering. Note that the blue line in both Figure 3.5 and Figure 3.6 is the combined data from multiple runs, which has been low-pass filtered after the combining to remove noise.

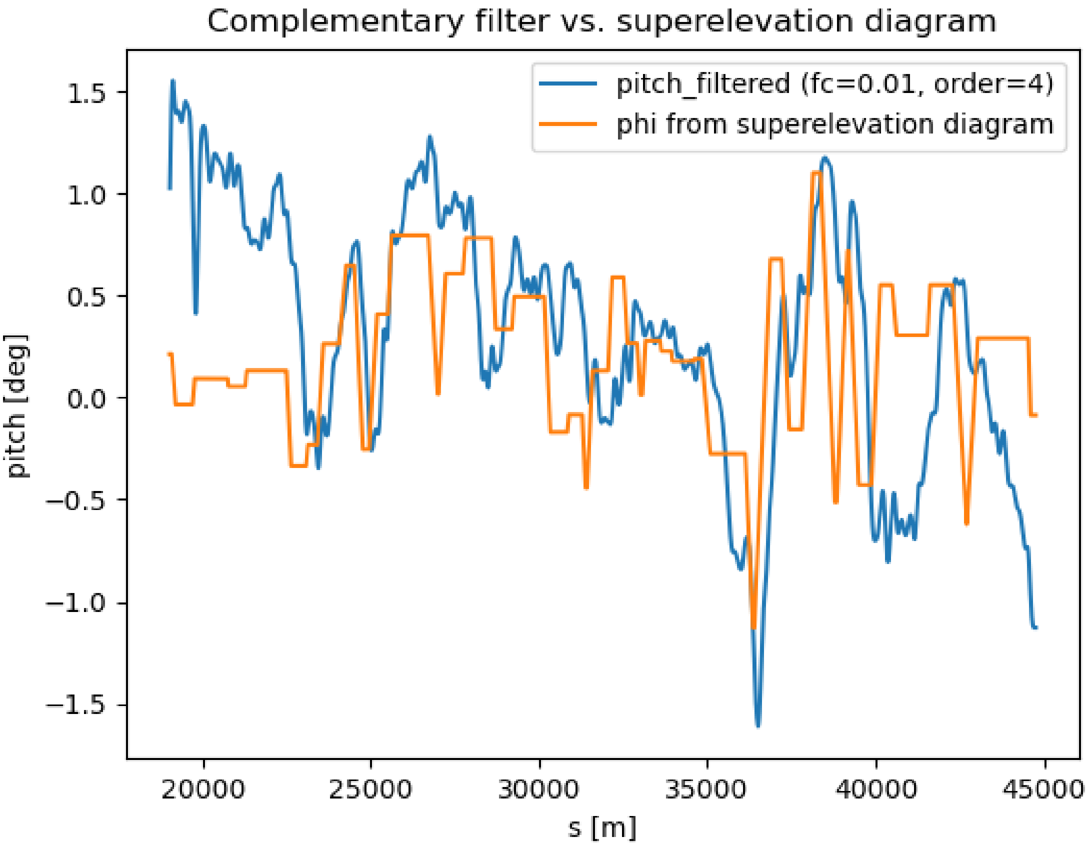

Figure 3.5: Comparison of the data calculated using a complementary filter and the pitch from the superelevation diagram

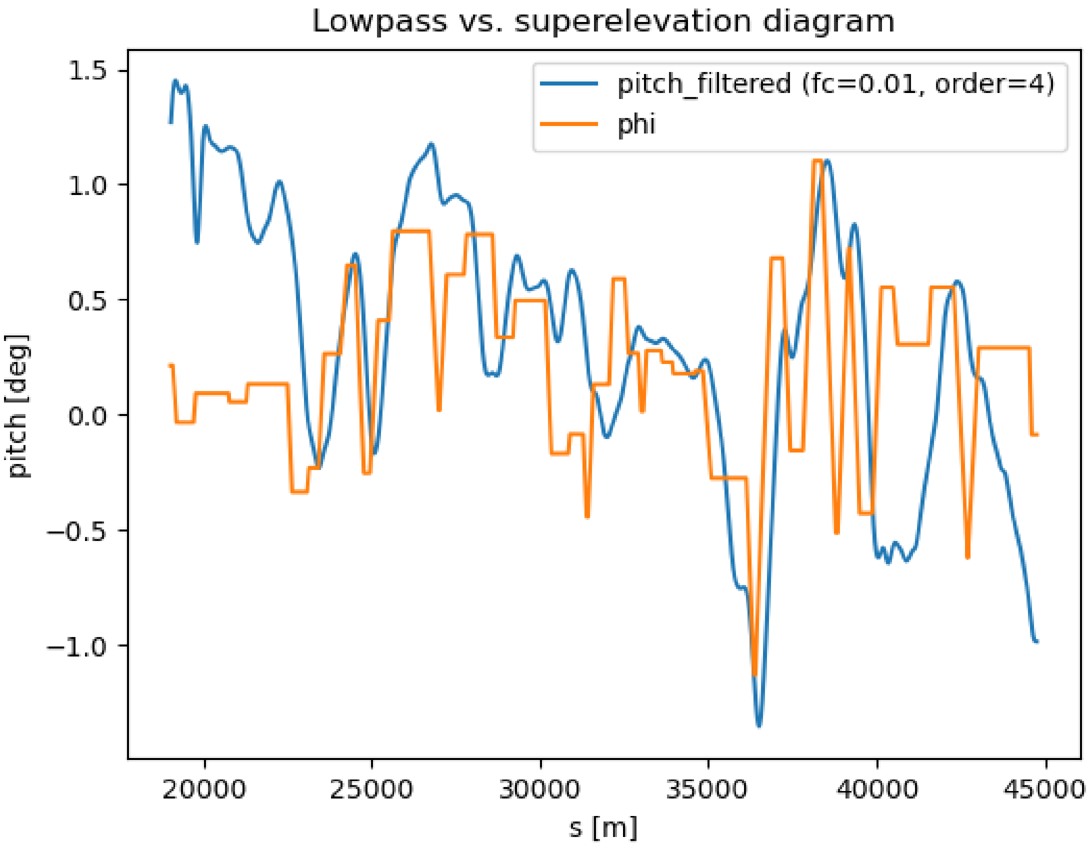

Figure 3.6: Comparison of the data calculated using a low-pass filter and the pitch from the superelevation diagram

Here, it can be observed that the data from the IMU follows the rough shape of the superelevation diagram, but has many errors. Both figures also look more or less the same, indicating that the complementary filter only uses the accelerometer, and there is no information in the gyroscope data. On the other hand, GNSS data shows a much better correlation than expected. As shown in Figure 3.7, it accurately follows the pitch angle of the superelevation diagram along the entire track.

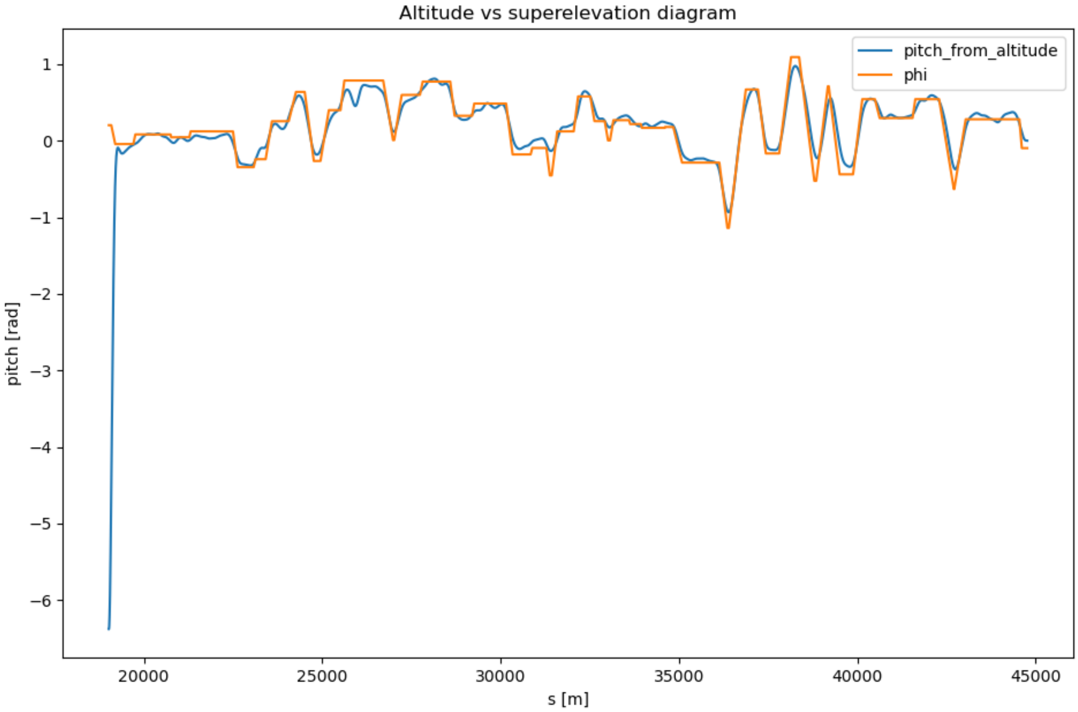

Figure 3.7: Comparison of the pitch angle calculated from altitude and the pitch from the superelevation diagram

3.3.1 Changes due to data quality

After evaluating the preliminary results and comparing the data from the IMU and the GNSS, some modifications to the original plan were made. It was decided to discard the data from the IMU and not attempt to fuse it with the GNSS data, opting to solely use the data from the GNSS. This decision was made since the IMU data contained less information than expected. There was no useful information in the gyroscope data, and the accelerometer data was noisier than anticipated.

3.3.2 Solution for data preparation

After considering the initial results gathered from the preprocessing, one method was singled out and used as the preprocessing step for the rest of the solution. This method uses only GNSS data. The preprocessing steps chosen are as follows:

1. Transform each run into the s-grid.
2. Calculate the median at each point for all the runs in the s-grid.
3. Filter the median along the s-grid using a low-pass filter to remove noise.

4 Clothoid generation

To represent the altitude of a railway in a standardized way, it must be represented using clothoid splines. To achieve this, splines must be fitted to the data generated by the preprocessing step. To achieve this, two different methods were tested: Random acquisition and random acquisition with sequential Monte Carlo. Both methods are adapted from Cemits prototype designed to operate in the xy-plane to work with altitude.

The clothoid splines used in railway and superelevation diagrams have an additional constraint they need to fulfill. This is to make the entire spline continuous with no breaks. Both the algorithms for generating clothoid splines abide by this constraint, which is:

$$c_{\theta_{end}}[i] = c_{\theta_{start}}[i+1]$$
$$c_{\kappa_{end}}[i] = \frac{d\theta}{ds}_{start}[i] = c_{\kappa_{end}}[i+1] = \frac{d\theta}{ds}_{start}[i+1]$$

where:

- $c_{\theta_{start}}$: Is the angle of the clothoid at the start.
- $c_{\theta_{end}}$: Is the angle of the clothoid at the end.
- $c_{\kappa_{start}}$: Curvature at the start of the clothoid.
- $c_{\kappa_{end}}$: Curvature at the end of the clothoid.

4.1 Random sample consensus

The random sample consensus (RANSAC)[23] method uses randomly selected points along the track and the altitude data at these points for the generation of clothoids[24]. It does this many times while keeping track of the best result. This algorithm is inspired by the same process used in image processing for aligning features in different images. The algorithm used here can be described using the following steps:

1. Randomly pick n points along the s-grid.
2. Compute the tangent at each point.

3. Generate a clothoid connecting each point, forming a spline.
4. Discretize the clothoid spline.
5. Calculate the RMSE between the spline and the dataset.
6. Store the clothoid spline if its RMSE is better than the current best.

This method relies heavily on the random points chosen by the random algorithm. The points should be distributed along the spline in addition to being random to form a good spline. Due to this, picking points completely at random is not suitable. This can lead to large stretches with no points and small stretches with clusters of points. Therefore, a slightly different approach was chosen to select the random points, which is as follows:

1. Create a vector of random values between 0 and 1 with the length of the desired amount of random points.
2. Take the cumulative sum of the vector.
3. Normalize this vector.
4. Scale the vector up to the length of the s-grid ($vector \cdot s_n$)

Figure 4.1 shows the a simplified version of the code used to generate the random points. This code generates a vector of 4 point on a stretch which is 10 meters long.

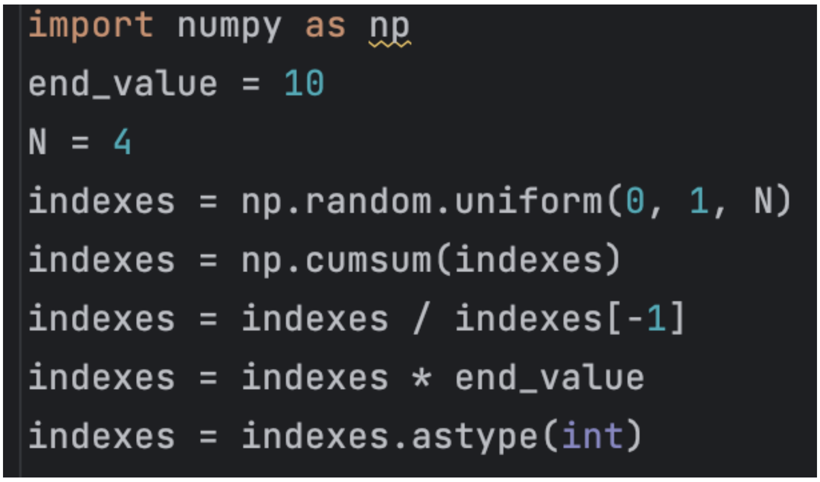

```
import numpy as np
end_value = 10
N = 4
indexes = np.random.uniform(0, 1, N)
indexes = np.cumsum(indexes)
indexes = indexes / indexes[-1]
indexes = indexes * end_value
indexes = indexes.astype(int)
```

Figure 4.1: Code for generating a vector of 4 points. Simplified for illustration purposes.

The tangents computed in step 2 are used as the start/end angles of clothoids in the spline. Using this, in addition to the position of the points in the s-grid, clothoids can be fitted between the points. This is done with an algorithm called G1 Hermite[25]. This algorithm takes in a start and an end point along with a start and end angle. With this information, it is able to numerically solve the interpolation, providing a clothoid as the result.

To validate the generated clothoid spline and see how well it matches the data, the spline must be resolved. This is done with the same resolution as the s-grid. Then the RMSE can be calculated between the spline and the dataset. This error is then used to determine if the spline is better than the current best and should be the new best or if it should be discarded.

This algorithm uses 2 tuning parameters which alter its behavior: N_clothoids and iterations. N_clothoids is the number of clothoids the spline should consist of, which in turn determines how many random points are generated. Iterations control how many times the algorithm runs; increasing this will increase the likelihood of a good solution being found at the expense of time.

4.2 Sequential Monte Carlo RANSAC

This algorithm is an extension of RANSAC, adding some extra randomness to the clothoid parameters and residual resampling using the Monte Carlo Sequential method[26]. The steps in the algorithm are the same as in chapter 4.1, except for step 3, where all the exceptions are implemented.

The first step is to generate a population of clothoids with size POP_SIZE from the first random point to the second using a normal distribution around the random points as the parameters for the clothoids. Then the weight for each is calculated using the root mean square between all these clothoids and a clothoid created using the G1 Hermit algorithm. Using the weights, the population is resampled using important sampling[27]. Lastly, the population is mutated, giving them new values for curvature and length randomly drawn from a normal distribution. This is how the first population of clothoids spanning from the first to the second random point in the s-grid is created. The subsequent clothoids in the spline are generated mostly the same, but with a few differences.

For the consecutive clothoids, the population is created with random values for only the end point, to ensure no breaks in the spline. Then the weights of the spline up to the current point are calculated using the root mean square between the population and a spline generated using the G1 Hermit algorithm. With the weights, the spline is resampled using a importent sampling. Lastly, the clothoid at the current end of the spline is mutated. This results in a population of splines growing from the start of the s-grid to the end. Figure 4.2 shows an illustration of this process, this shows the result after fitting only the first 4 clothoids. the red line is the clothoid generated using G1 Hermit, the dotted lines are the clothoid is the population and the green/red dots are the star/end points of a clothoid segment.

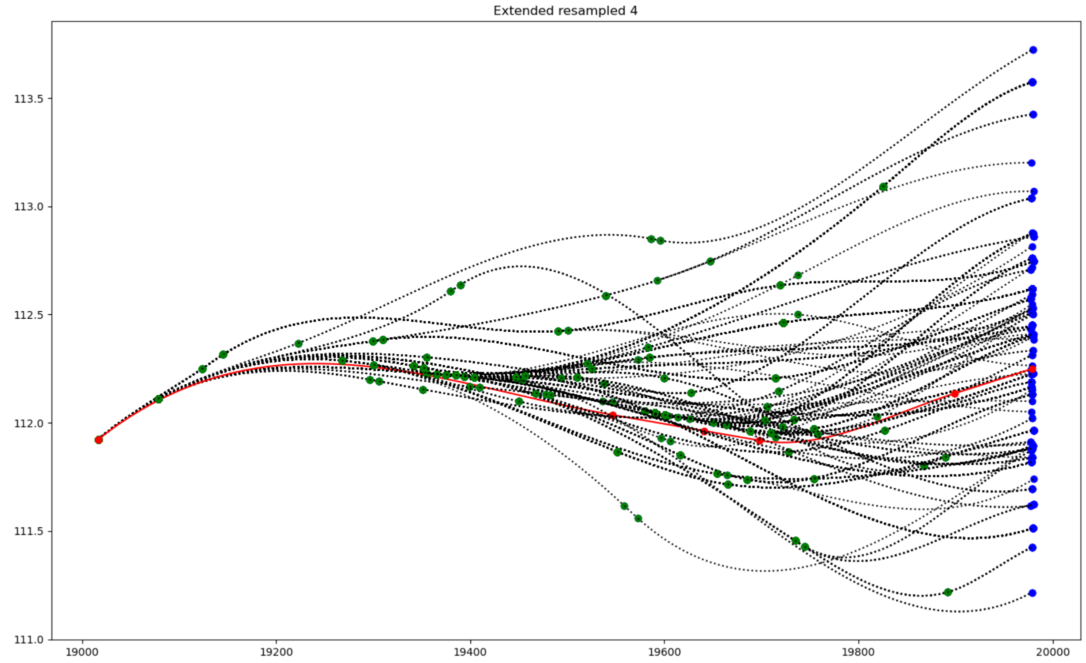

Figure 4.2: Resulting population of clothoids after 4 iterations of fitting clothoids.

This algorithm uses 4 additional tuning parameters in addition to the 2 used in the random acquisition 4.1 algorithm. These are 3 σ values and population_size. σ_θ, σ_l, and σ_k are used to control the width of the random distribution for getting the angle, length, and curvature of the clothoids. Population size is used to determine the size of the clothoid population generated.

4.3 Brute force local gradient decent

The likelihood of the algorithms described in 4.1 and 4.2 producing an optimal result is close to zero. Hence, the result can likely be improved upon using an optimization algorithm. The optimization algorithm tested is a simple brute force algorithm. It moves the randomly generated points one by one and checks if the error improves. The pseudocode in Listing 4.1 shows the working principle of this algorithm.

```
for i in iterations:
    for p in points:
        move_point_left(p)
        Calculate_target(p)
        recompute_spline()
        calculate_error()

        if new_error < old_error:
            accept_move()
        else:
            recject_move()

            move_point_right(p)
            Calculate_target(p)
            recompute_spline()
            calculate_error()
            if new_error < old_error:
                accept_move()
            else:
                recject_move()
```

Listing 4.1: Pseudo code illustrating the search algorithm

5 Results

This section presents the various results obtained from generating superelevation diagrams using data from multiple train runs. The outcomes from the preprocessing step and associated uncertainties in the data are discussed. Additionally, the resulting clothoid splines generated using different methods are shown and compared, both with and without optimization.

5.1 GNSS dataset

Using data gathered over a period of 4 months, approximately 900 runs over the given stretch of track were acquired. By combining all these runs, a dataset containing the average height of the track can be created. Figure 5.1 shows the median and the average of all the altitudes at each point, in addition to the median filtered and the data from the superelevation diagram. The collected data follows the general shape of the superelevation diagram but has some bias errors on parts of the stretch. It can also be observed that there are some anomalies with the collected data at the start. The sharp drop of approximately 10 meters is unlikely and may be a result of uncertainties due to poor GNSS satellite coverage in that area.

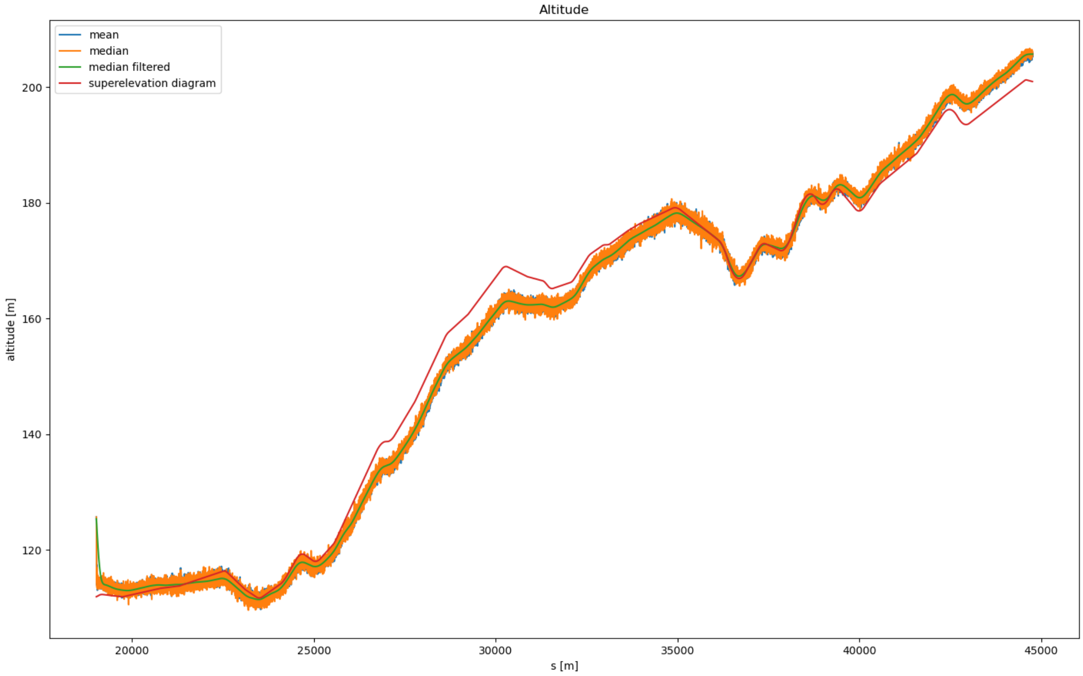

Figure 5.1: Measured altitude of the track

5.1.1 Uncertainty in the dataset

The dataset contains a few different sources of uncertainty which needs do be explained to give context to the results. This chapter will explain the different sources of uncertainty present in the dataset.

GNSS measurement uncertainty

GNSS measurements are subject to the the phenomena called dilution of precision which affects the uncertainty of the measurements[28]. GNSS divides this into to parts horizontal dilution of precision (Hdop) and vertical dilution of precision (Vdop)[29]. Whit this values the uncertainty's of the measurements can be calculated. Unfortunately sins the CDC wasn't intended to be used for this purpose the Vdop value has not been recorded, which makes the uncertainty of the measurement doe to dilution of precision hard to find.

Even though Vdop would increase the estimate of uncertainty, an estimate can still be found. Calculating the standard deviation for each point in the s-grid provides an estimate of the spread of the altitude measurements. Figure 5.2 shows the standard deviation σ for each meter in the s-grid. The trend-line is around 5 meters, and the variations are probably due to differing receiver conditions along the track. From this, an estimate for the average sigma can be calculated, which is: 5.1 meters. This is within what can be expected from GNSS, as shown in Table 13 in "An Introduction to GNSS" [30].

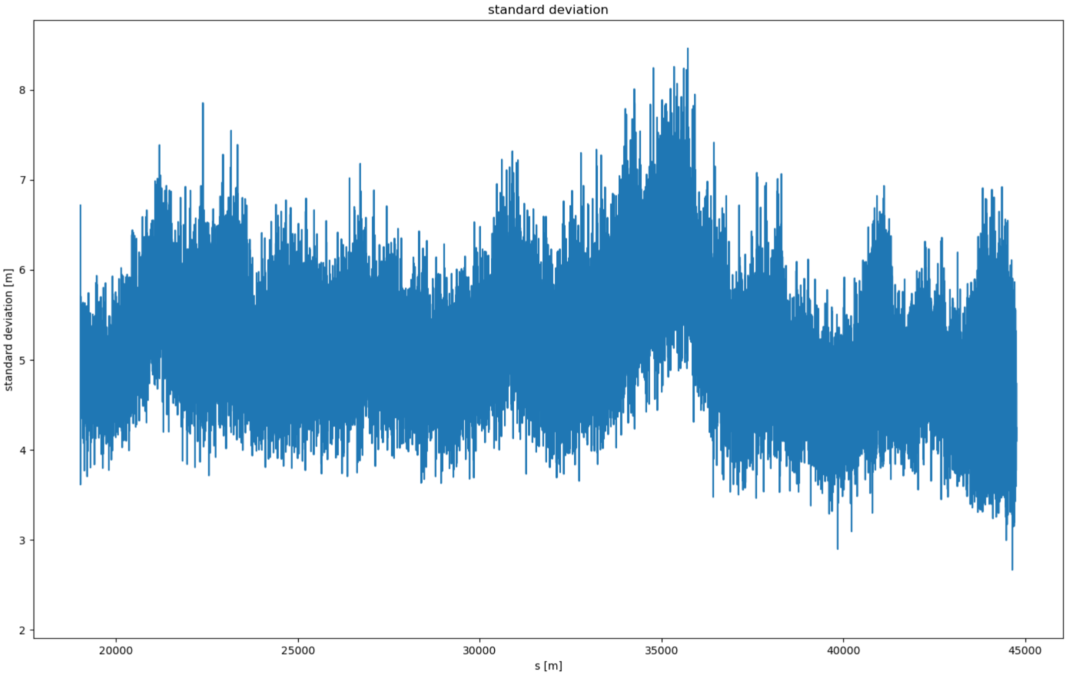

Figure 5.2: Standard deviation at each point in the s-grid.

Accuracy of superelevation diagram

The superelevation diagram is the technical specification of how the railway was built, hence it can be used as a reference to evaluate the result. However, due to the age of most of the superelevation diagrams, they contain varying amounts of errors and misalignments. This is mostly due to changes doe to ground movement that have not been reflected in the diagram. To combat this and make the superelevation diagram usable as a reference, they have been manually corrected. This has been done manually in-house at Cemit with some help from local technicians working on the railway. Hence, the superelevation diagram used is not a perfect representation of the railway and contains some misalignments.

Since the superelevation diagram is a set of clothoids originating from a point, it is also prone to integration error. The diagram used is discretized by integrating over these clothoids. Due to this integration, which is over a distance of 45 km, the result is susceptible to small errors propagating. In Norway, all superelevation diagrams have the same starting point, which is approximately at Oslo Central Station. The point is not exact and is a source for more inaccuracies. In other words, the initial conditions for the integration are not precisely known and are approximated using a map.

5.2 Clothoid generation

Generation of clothoid is done using to different methods inspired by RANSAC. Both uses data form the GNSS senor ant try to fit a clotoid spline to it. This chapter will evaluate the result form both this method and see how they compare. In addition the brute force local gradient decent optimisation algorithm will be tested to see if the rerults improve.

5.2.1 Random sample consensus

The RANSAC algorithm is able to produce a spline that fits the dataset quite well. It consistently produces a result with an RMSE below 1 meter even when run with relatively few iterations. However, it seems to have a soft cap around 0.2 meter in RMSE, struggling to get below this error. Running this algorithm with 1000 iterations and 50 clothoids produces the result shown in Figure 5.3. The blue line is the superelevation diagram for the stretch, the purple line is the clothoids generated, and the green line is the dataset. The green dots are the points used to calculate the clothoids.

From trial and error, it seems that fewer clothoids produce a better result. This stretch of track is composed of 85 clothoids according to the superelevation diagram, but inserting this many clothoids consistently produces a worse result than inserting 50.

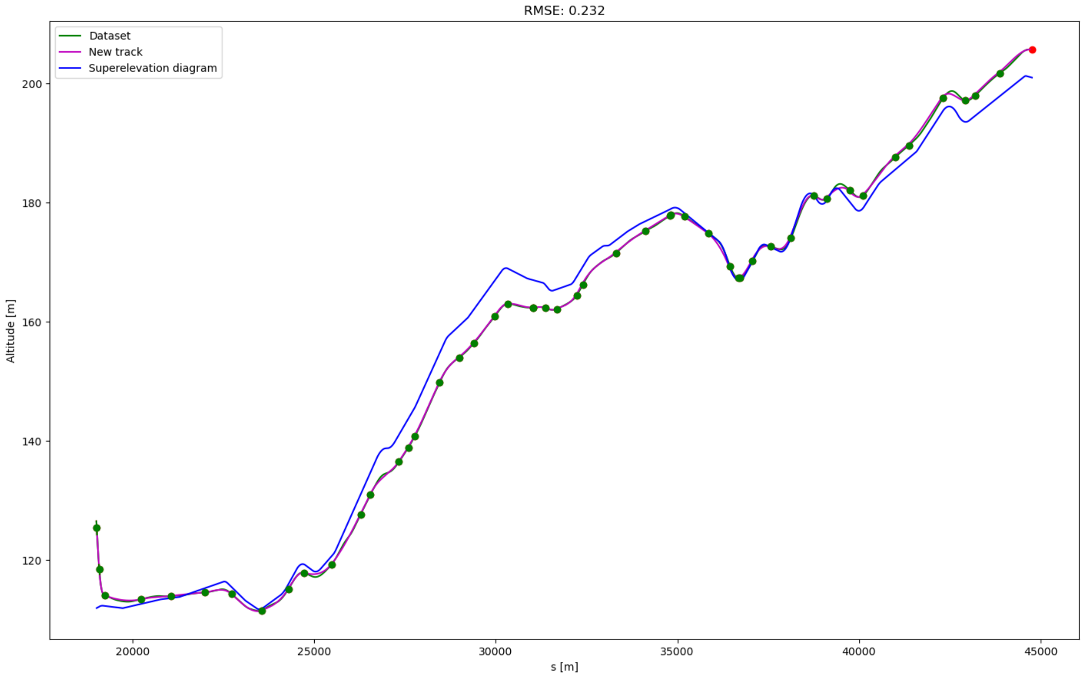

Figure 5.3: Resulting clothoid spline using 1000 iterations and 50 clothoids on the dataset.

As a test, the algorithm was run with the discretized superelevation diagram as input. This is a perfect clothoid spline, so in theory, it should be possible to get an RMSE of 0 meter using the same number of clothoids as the superelevation diagram, which is 85. As shown in Figure 5.4, this was not the case, and the result is worse than with 50 clothoids. This is probably due to many of the points used to generate the clothoids ending up very close to each other, providing no information, as shown in Figure 5.5. Here, the three points on the straight part are redundant and provide no additional information.

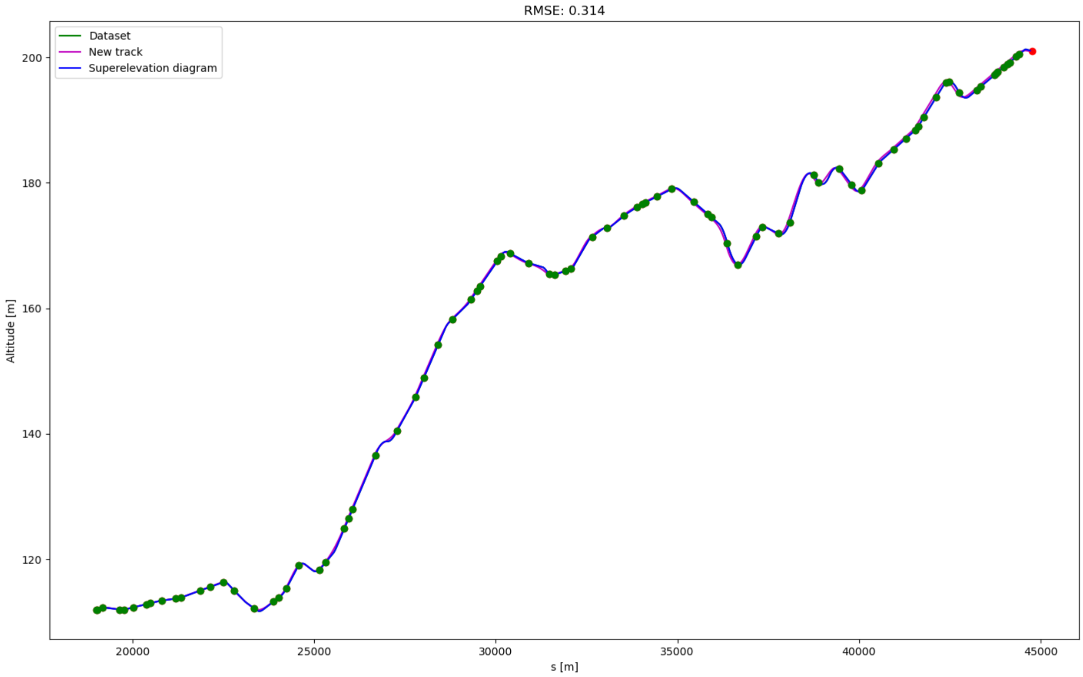

Figure 5.4: Resulting clothoid spline using 1000 iterations and 85 clothoids on the discretized superelevation diagram.

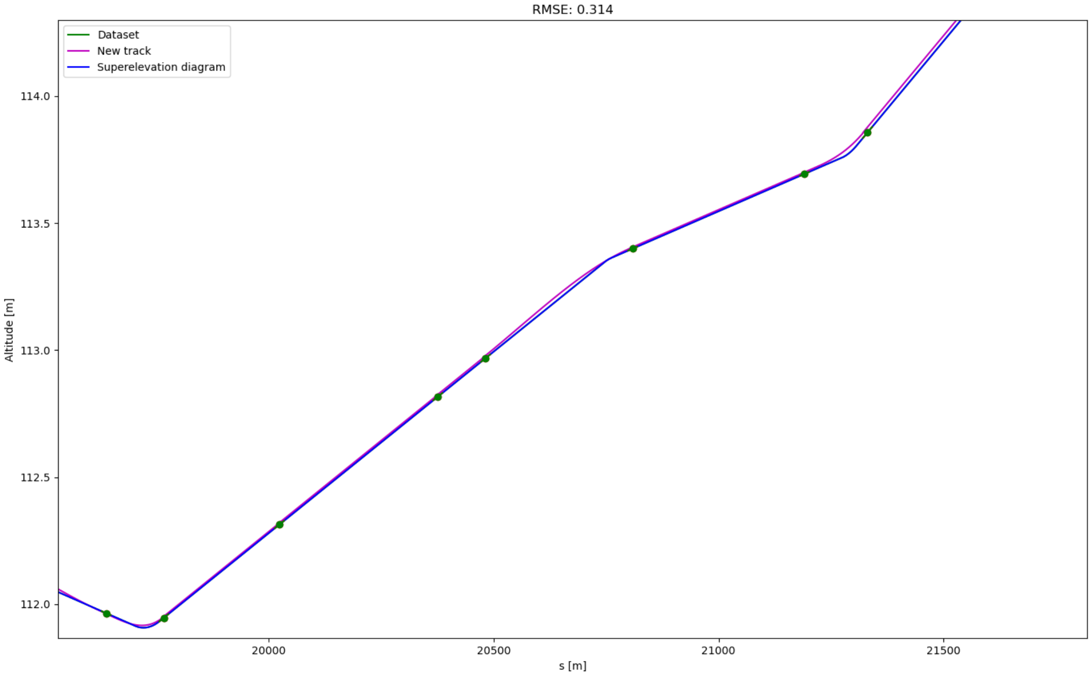

Figure 5.5: Close up of Figure 5.4 showing the redundant points.

5.2.2 Random sample consensus Monte Carlo

The algorithm with Monte Carlo sampling performed worse than expected. It consistently underperformed the one without. This is probably due to the algorithm originally being designed for generating 2D superelevation diagrams in the latitude/longitude space. The algorithm places the start and end points of the clothoid around the generated point, which is on the line from the dataset. This is to account for the dataset not being perfect, but will give a worse RMSE when it is compared to the dataset.

This algorithm also has more tuning parameters, making it more complex to tune. This algorithm is probably not tuned well enough, and is also one of the reasons for its worse performance. Figure 5.6 shows the result from this algorithm using 50 clothoids, 100 iterations, and a population size of 1000. The σ values are as follows: $\sigma_x = 1$, $\sigma_y = 1$, $\sigma_\theta = 0.0002$, $\sigma_k = 0.00001$ and $\sigma_l = 300$. Here, the green line is the dataset, the purple line is the generated clothoid spline, and the blue line is the superelevation diagram. The green dots are the randomly generated points, while the red dots are the start/end points of each clothoid after the Monte Carlo sampling.

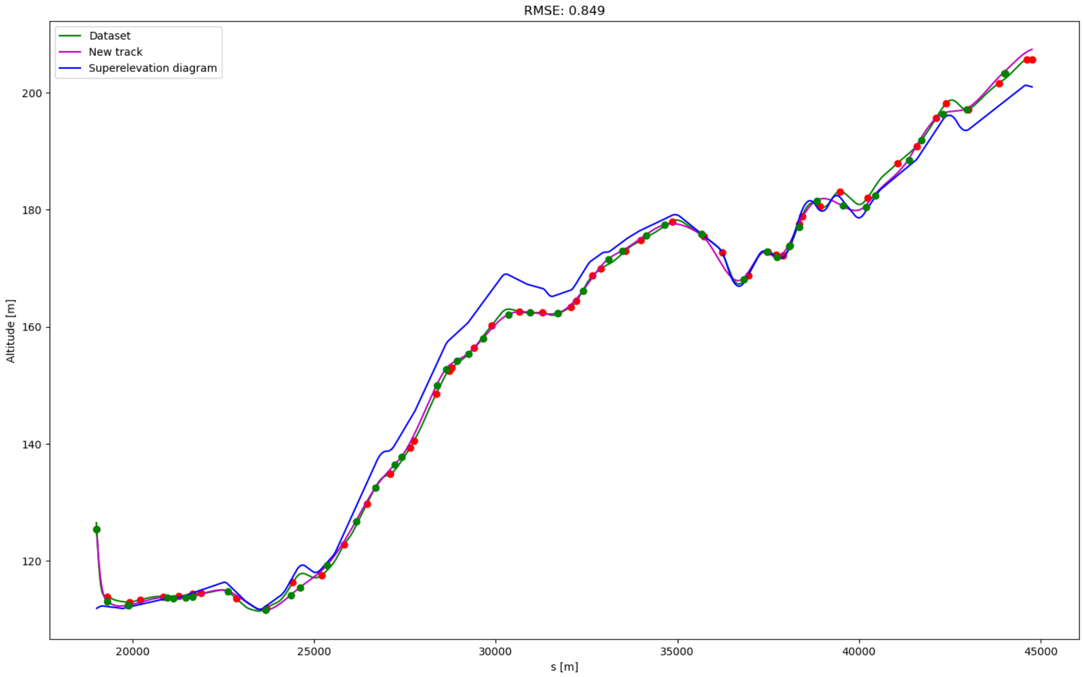

Figure 5.6: Resulting clothoid spline using 100 iterations, 50 clothoids, and a population of 1000 on the dataset.

Running this algorithm using the discretized superelevation diagram as input produces similar results and consistently performs worse than the algorithm not using Monte Carlo sampling. However, this algorithm improves its result using more clothoids. One reason for this might be that the Monte Carlo sampling spreads out the points, increasing the likelihood of them containing useful information. Figure 5.7 shows the result from running the algorithm with the discretized superelevation diagram as input and 85 instead of 50 clothoids.

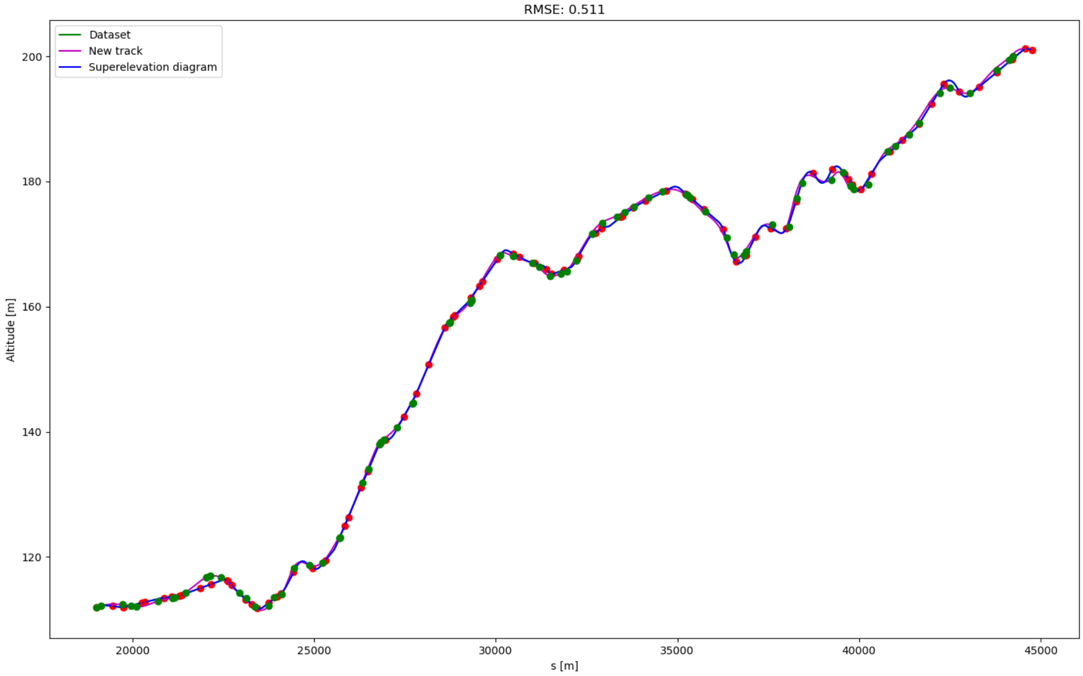

Figure 5.7: Resulting clothoid spline using 100 iterations, 85 clothoids, and a population size of 1000 on the discretized superelevation diagram.

5.2.3 Brute force local gradient decent

This optimization algorithm was intended to be used on the results from both the algorithms for generating clothoids. However, due to the complexity of the Monte Carlo algorithm, the implementation was not straightforward. Due to this and time constraints, the optimization was only tested on the simpler algorithm, which only uses RANSAC.

On a clothoid spline consisting of 50 clothoids, the optimization is able to decrease the RMSE slightly from 0.253 meter to 0.189 meter. This is a small improvement, confirming that this simple approach to improving the result works. However, significantly smaller errors are starting to become unlikely due to the error caused by discretization when calculating RMSE. Figure 5.8 shows the small improvement caused by the optimization. The figure is zoomed for the change to be noticeable.

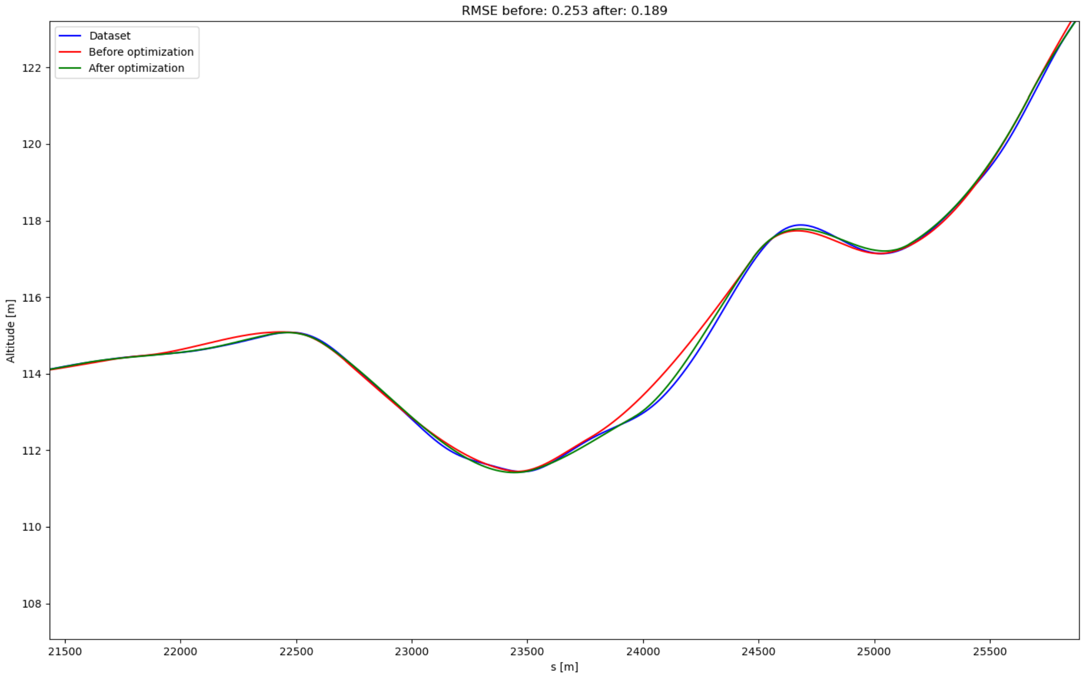

Figure 5.8: Comparison between before and after optimization.

As a test, the optimization algorithm was run on a spline using the superelevation diagram as the input, with 85 as the amount of clothoids. This is to see if, with optimization, it is possible to recreate the superelevation diagram. As shown in Figure 5.9, the result is on par with running the algorithm with 50 clothoids without optimization. This may indicate that the optimization algorithm does not handle clusters of points well due to its simplicity.

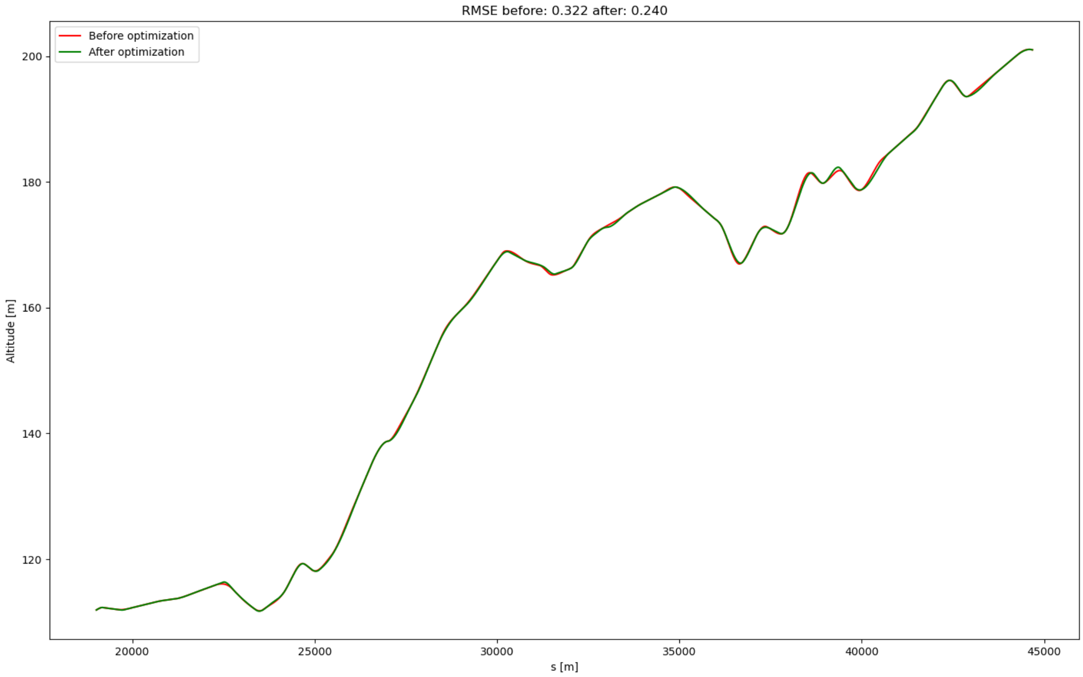

Figure 5.9: Comparison between before and after optimization using the superelevation diagram as input.

6 Discussion

This chapter will discuss the performance of the solution and whether it is able to perform its intended task. The impact of different uncertainties on the solution and their effects on performance will also be discussed. The various approaches taken and discarded during the preprocessing will be examined as well.

6.1 Preprocessing

The original plan for this solution was to use an IMU sensor in combination with a GNSS sensor to predict the elevation of a stretch of railroad track. However, after examining the initial results after filtering the IMU data, the decision to exclude IMU was made. This was due to the poor results from the filtering. The results showed that there was some information in the signal, but there was also a lot of noise. The hypothesis before the work started was that the combination of a gyroscope could provide a good estimate of the orientation of the train and hence the track. The results from the GNSS sensor, on the other hand, were better than expected. With this in mind, the decision of excluding the IMU sensor was taken. It is acknowledged that this could have been concluded before the project started by looking at the data, but such a study was not conducted.

The data from the GNSS sensor looked promising. It produced promising results even when combining smaller amounts of runs. It also improved in performance by combining larger amounts of runs up to a point, and then the improvement stagnated. Due to this, a larger dataset of about 900 runs from a timespan of 4 months was chosen.

6.1.1 Uncertainties in the dataset

The accuracy and precision of the dataset used are difficult to validate due to a lack of a reliable reference. The superelevation diagram is supposed to be this reference, but it is a poor one. This is because the superelevation diagram used as a reference for this stretch of track is known to have faults. The faults have been corrected manually but not verified properly. In addition, the starting point for the spline in the diagram is only a guess made using a map. Since the spline in the superelevation diagram must be discretized, small errors like this can have a large impact.

The GNSS data also appear to have low precision, and the measurements vary a lot from run to run. This makes it so the actual true altitude is unknown and probably lies somewhere between the value from the dataset and the value from the superelevation diagram. Hence, a validation of the dataset against a trustworthy source is needed to evaluate if the dataset reflects reality.

6.2 Clothoid generation

Both algorithms for generating clothoids worked and were able to produce a spline following the dataset. The simpler RANSAC method was the best to follow the dataset and therefore had the lowest RMSE, but the Monte Carlo algorithm also performed well. The Monte Carlo algorithm was probably not tuned well enough and could have performed better with better tuning of all the parameters. Both algorithms performed best with fewer clothoids than the track has. This is probably due to how the random points are generated. With larger amounts of points, they tended to cluster together at some smaller stretches and leave longer stretches without any points. This issue is probably solvable by distributing the points in a smarter way and could improve the performance while using larger amounts of points.

Using the simpler RANSAC algorithm with optimization performed the best only looking at the error. This managed to consistently achieve below 0.2 meter in RMSE, showing that the algorithm is capable of fitting a spline to the dataset with pretty good accuracy. However, problems with evaluating the result against a reference arise here as well. Due to this, the best the algorithm can be expected to do is to fit a spline to the data it is given. Then the result is mainly dependent on how well the input data matches reality.

6.3 Fusion of IMU and GNSS

The research started with the goal of using both IMU and GNSS to produce an elevation profile of a stretch of railway track. However, this was never attempted due to the poor results from the IMU. As has been shown, only GNSS data is able to produce an elevation profile, but it cannot be better than the accuracy of GNSS, which is around 5 meters. This can probably be improved using sensor fusion with another type of sensor better suited for measuring small elevation angles. One candidate for such a sensor is the ”Electrolytic Tilt Sensor” [31], which measures angles directly. Another solution that can be considered is fusing data from an atmospheric pressure sensor with the altitude measured from GNSS [32].

7 Conclusion

In this thesis, we have investigated the feasibility of accurately predicting the elevation of a stretch of railroad track using a combination of sensors, data processing techniques, and algorithms. Although the initial approach considered using an IMU sensor alongside a GNSS sensor, the results prompted a change in direction, excluding the IMU sensor due to its noise and filtering issues. The focus was then shifted to preprocessing the data, examining uncertainties in the dataset, and generating clothoid splines that best fit the data.

The results of our investigation indicate that the simpler RANSAC algorithm, when combined with optimization, was able to consistently achieve an RMSE below 0.2 meter. This demonstrates the algorithm's ability to fit a spline to the dataset with reasonable accuracy. However, the true performance of the solution is primarily dependent on the quality of the input data and its alignment with the actual elevation values.

Throughout the course of this study, several challenges were encountered, such as the distribution of points in the clothoid generation process and the lack of a trustworthy reference for validating the dataset. These challenges highlight the potential areas for improvement in future work.

One possible avenue for future research is the exploration of different sensor types to enhance the quality of the elevation estimates. By fusing data from other sensors, such as atmospheric pressure sensors or electrolytic tilt sensors, the accuracy of the predictions may be further improved.

In conclusion, this thesis demonstrates that it is possible to accurately predict the elevation of a stretch of railroad track using a combination of sensors and data processing techniques. However, it also emphasizes the need for further research to address the limitations and uncertainties identified in this work. By refining the methodologies, algorithms, and data processing techniques, we believe that the performance of the solution can be significantly improved, paving the way for a more reliable and accurate prediction of railroad track elevation.

7.1 Further Work

There are several areas where future research can be conducted to enhance the accuracy and reliability of the elevation prediction for railroad tracks. Some potential directions for further work include:

- **Sensor Fusion:** Investigate the use of other sensors, such as atmospheric pressure sensors or electrolytic tilt sensors, in combination with GNSS data to improve the elevation estimation. Fusing data from different sensors could lead to more accurate results and compensate for the limitations of individual sensors.
- **Optimization of Clothoid Generation Algorithms:** Enhance the performance of the clothoid generation algorithms by optimizing the distribution of points or tuning the parameters more effectively. This could result in better fitting splines and reduced errors in elevation prediction.
- **Validation Against Trustworthy References:** Establish a more reliable reference dataset for validating the elevation estimates. This could involve using high-precision surveying equipment or other methods to obtain accurate ground truth data for the elevation of the railroad track.
- **Evaluating Alternative Algorithms:** Explore alternative algorithms and approaches for generating elevation profiles of railroad tracks. Comparing the performance of various methods could reveal new insights and help identify the most effective techniques for this application.

By addressing these areas in future research, the performance of the elevation prediction solution can be significantly improved, leading to more accurate and reliable estimates for railroad track elevation.

7.2 Acknowledgements

I would like to extend my gratitude to my supervisor, Håkon Viumdal and Ole Magnus Brastein, for their guidance, support, and valuable suggestions during the course of this thesis. Their expertise and dedication have been essential in shaping the direction and outcome of this research.

I also appreciate the team at Cemit for providing me with the resources and facilities required to carry out this study. Their assistance and encouragement have been crucial to the successful completion of this work.

Bibliography

[1] P. Weston, C. Roberts, G. Yeo and E. Stewart, 'Perspectives on railway track geometry condition monitoring from in-service railway vehicles,' eng, *Vehicle system dynamics*, vol. 53, no. 7, pp. 1063–1091, 2015, ISSN: 0042-3114.

[2] ENSCO, *Rack geometry measurement systems (*, Last accessed 11 APR 2023, 2023. [Online]. Available: `https://www.ensco.com/rail/track-geometry-measurement-system-tgms`.

[3] E. Aldao, H. González-Jorge, L. M. González-deSantos, G. Fontenla-Carrera and J. Martínez-Sánchez, 'Validation of solid-state lidar measurement system for ballast geometry monitoring in rail tracks,' eng, *Infrastructures (Basel)*, vol. 8, no. 4, p. 63, 2023, ISSN: 2412-3811.

[4] S. Wang, G. Liu, G. Jing, Q. Feng, H. Liu and Y. Guo, 'State-of-the-art review of ground penetrating radar (gpr) applications for railway ballast inspection,' eng, *Sensors (Basel, Switzerland)*, vol. 22, no. 7, p. 2450, 2022, ISSN: 1424-8220.

[5] J. G. Hook, 'Fundamentals of railway curve superelevation,' 2017. [Online]. Available: `https://www.jghtech.com/assets/applets/LFLSRM-Fundamentals-of-Railway-Curve-Superelevation-current.pdf`.

[6] InvenSense, *Mpu-6000 and mpu-6050 product specification revision 3.4*, Last accessed 4 MAY 2023, 2013. [Online]. Available: `https://invensense.tdk.com/wp-content/uploads/2015/02/MPU-6000-Datasheet1.pdf`.

[7] Quectel, *Iot/m2m-optimized lte cat 4 module*, Last accessed 4 MAY 2023, 2023. [Online]. Available: `https://docs.rs-online.com/c01f/A700000007115515.pdf`.

[8] J. G. Hook, 'Fundamentals of railway curve superelevation,' Apr. 2018. [Online]. Available: `https://www.jghtech.com/assets/applets/LFLSRM-Fundamentals-of-Railway-Curve-Superelevation-current.pdf`.

[9] S. Judek, A. Wilk, W. Koc *et al.*, 'Preparatory railway track geometry estimation based on gnss and imu systems,' *Remote Sensing*, vol. 14, no. 21, 2022, ISSN: 2072-4292. DOI: `10.3390/rs14215472`. [Online]. Available: `http://dx.doi.org/10.3390/rs14215472`.

[10] S. Rehman, M. F. Khan, H.-D. Kim and S. Kim, 'Energy-efficient and reconfigurable complementary filter based on analog–digital hybrid computing with sns2 memtransistor,' eng, *Nano energy*, vol. 109, 2023, ISSN: 2211-2855.

[11] P. Narkhede, S. Poddar, R. Walambe, G. Ghinea and K. Kotecha, 'Cascaded complementary filter architecture for sensor fusion in attitude estimation,' 2021.

[12] E. G. Hemingway and O. M. O'Reilly, 'Perspectives on euler angle singularities, gimbal lock, and the orthogonality of applied forces and applied moments,' eng, *Multibody system dynamics*, vol. 44, no. 1, pp. 31–56, 2018, ISSN: 1384-5640.

[13] M. Euston, P. Coote, R. Mahony, J. Kim and T. Hamel, 'A complementary filter for attitude estimation of a fixed-wing uav,' Oct. 2008, pp. 340–345. DOI: `10.1109/IROS.2008.4650766`.

[14] D. Kumar, 'Comparison of different types of iir filters,' Apr. 2016. DOI: `10.13140/RG.2.1.4856.3605`.

[15] B. Technologies, *Filter topology face off: A closer look at the top 4 filter types*, Last accessed 18 APR 2023, 2016. [Online]. Available: `https://blog.bliley.com/filter-typology-face-off-a-closer-look-at-the-top-4-filter-types`.

[16] 1. Analog Circuits Cookbook (Second Edition), *Butterworth filter*, Last accessed 8 MAY 2023, 1999. [Online]. Available: `https://www.sciencedirect.com/topics/engineering/butterworth-filter`.

[17] 2. Linear Circuit Design Handbook, *Bessel filter*, Last accessed 8 MAY 2023, 2008. [Online]. Available: `https://www.sciencedirect.com/topics/engineering/bessel-filter`.

[18] M. m. t. Elahe Hamidi, 'Improvements in the transient response of distributed amplifiers,' Oct. 2007. [Online]. Available: `https://www.researchgate.net/publication/31205574_Improvements_in_the_Transient_Response_of_Distributed_Amplifiers`.

[19] Scipy, *Scipy.signal.filtfilt*, Last accessed 18 APR 2023, 2023. [Online]. Available: `https://docs.scipy.org/doc/scipy/reference/generated/scipy.signal.filtfilt.html`.

[20] P. MarcinLigas, 'Conversion between cartesian and geodetic coordinates on a rotational ellipsoid by solving a system of nonlinear equations,' Apr. 2011. [Online]. Available: `https://journals.pan.pl/Content/98324/PDF/art05.pdf`.

[21] GeographicLib, *Geographiclib.geodesic*, Last accessed 18 APR 2023, 2023. [Online]. Available: `https://geographiclib.sourceforge.io/Python/doc/code.html#module-geographiclib.geodesic`.

[22] K. Betke, 'The nmea 0183 protocol,' Jul. 2001. [Online]. Available: `https://www.tronico.fi/OH6NT/docs/NMEA0183.pdf`.

[23] O. Chum and J. Matas, 'Optimal randomized ransac,' eng, *IEEE transactions on pattern analysis and machine intelligence*, vol. 30, no. 8, pp. 1472–1482, 2008, ISSN: 0162-8828.

[24] T. Opsahl, *Robust estimation with ransac*, Last accessed 4 MAY 2023, 2023. [Online]. Available: https://www.uio.no/studier/emner/matnat/its/nedlagte-emner/UNIK4690/v16/forelesninger/lecture_3_3-robust-estimation-with-ransac.pdf.

[25] D. Meek and D. Walton, 'A two-point g1 hermite interpolating family of spirals,' *Journal of Computational and Applied Mathematics*, vol. 223, no. 1, pp. 97–113, 2009, ISSN: 0377-0427. DOI: https://doi.org/10.1016/j.cam.2007.12.027. [Online]. Available: https://www.sciencedirect.com/science/article/pii/S0377042707006711.

[26] J. S. Liu and R. Chen, 'Sequential monte carlo methods for dynamic systems,' *Journal of the American Statistical Association*, vol. 93, no. 443, pp. 1032–1044, 1998, ISSN: 01621459. [Online]. Available: http://www.jstor.org/stable/2669847 (visited on 27/04/2023).

[27] v. d. M. R. Elfring J Torta E, 'Particle filters: A hands-on tutorial,' *National Library of Medicine*, 2021. [Online]. Available: https://www.ncbi.nlm.nih.gov/pmc/articles/PMC7826670/.

[28] R. B. Langley, 'Dilution of precision,' *GPS World*, 1999. [Online]. Available: http://gauss.gge.unb.ca/papers.pdf/gpsworld.may99.pdf.

[29] J. V. Sickle, *The space segment: Dilution of precision*, Last accessed 28 APR 2023, 2023. [Online]. Available: https://www.e-education.psu.edu/geog862/node/1771.

[30] N. inc, 'An introduction to gnss,' 2015. [Online]. Available: http://arf.berkeley.edu/files/attachments/equipment/NovAtel-Intro-to-GNSS2015.pdf.

[31] W. B. Powell, 'The electrolytic tilt sensor,' 2000. [Online]. Available: https://www.fierceelectronics.com/components/electrolytic-tilt-sensor.

[32] S. A. L. Crisóstomo, P. Auxiliar and F. de Ciências, 'Gnss and barometric sensor fusion for altimetry applications,' 2018. [Online]. Available: https://core.ac.uk/download/pdf/302954298.pdf.

[33] S. Sharma, Y. Cui, Q. He, R. Mohammadi and Z. Li, 'Data-driven optimization of railway maintenance for track geometry,' eng, *Transportation research. Part C, Emerging technologies*, vol. 90, pp. 34–58, 2018, ISSN: 0968-090X.

Appendix A

Task description

University of
South-Eastern Norway

Faculty of Technology, Natural Sciences and Maritime Sciences, Campus Porsgrunn

FMH606 Master's Thesis

Title: Vertical track geometry identification from IMU data

USN supervisor: Håkon Viumdal, Ole Magnus Brastein

External partner: CEMIT (Sigurd Aanesen)

Task background:

CEMIT is a company that develops technology to digitalize railways. To create intelligent railway systems, good mathematical representation of the tracks is crucial. Today, the layout of the tracks are described using superelevation diagrams, which are mathematical representations of the tracks using clothoid splines. The spline originates form a known position, which in Norway is by definition Oslo Central Station. The prevailing Norwegian superelevation diagram provides a good representation of the curves in three dimensions. However, the exact positions of the points along the track are not described in this model. The superelevation diagrams are originally designed for the construction purpose. Due to wear and tear and various whether conditions during the seasons, the track may be altered in different directions, so a system to monitor the changes of the tracks are desired.

Cemit has already created a solution for recreating superelevation diagrams form GNSS data, but this solution does not take elevation into account. The solution assumes that the track is on a completely flat surface. Cemit wants to explore the possibility to use elevation data form GNSS in combination with an IMU-sensor located at a train to improve this solution and incorporate vertical geometry.

Task description:

1. Describe how monitoring of railway tracks are done today, and potential solutions found in the literature. Emphasize the location and geometry of the tracks.
2. Describe Cemit's current solution for calculating the 2D geometry of the railway tracks, based on superelevation diagrams, geometry and GNSS data.
3. Describe how the drone technology or similar technology are using GNSS data to estimate the position and the track of a drone. Elaborate on how parts of this technology could potentially be implemented together with the superelevation diagram of railways to describe an updated 3D-version the railway track.
4. Preform an exploratory data analysis of the IMU data from train route to determine the quality of the data. Is the SNR sufficient for the shallow angels and angular velocities of a railway track?
5. Suggest and evaluate different methods for improving the elevation data from GNSS using gradient data form the IMU.
6. Try to estimate the vertical track geometry using data form IMU and GNSS on a train route with known gradient data. Compare the results.
7. Elaborate on how this solution can be combined whit the existing solution form generating superelevation diagrams.

Student category: Reserved for Industry master student in Industrial IT and Automation, Ruben Svedal Jørundland

Is the task suitable for online students (not present at the campus)?
The student is employed at CEMIT, and will mainly work in their office

Practical arrangements:
The student will need to organize access to relevant dataset as a part of his Master thesis, with support from CEMIT, if needed. That may include access to a track changer to run own experiment

Supervision:
As a general rule, the student is entitled to 15-20 hours of supervision. This includes necessary time for the supervisor to prepare for supervision meetings (reading material to be discussed, etc).

Signatures:

Supervisor (date and signature):

Student (write clearly in all capitalized letters): Ruben Svedal Jørundland

Student (date and signature): Ruben S. J